

COMPOSITE POLYTROPE MODELS OF MOLECULAR CLOUDS. I. THEORY

CHARLES L. CURRY^{1,2}

Astronomy Department, University of California, Berkeley, CA 94720

AND

CHRISTOPHER F. MCKEE

Departments of Physics and Astronomy, University of California, Berkeley, CA 94720

Draft version April 2, 2018

ABSTRACT

We construct spherical, hydrostatic models of dense molecular cores and Bok globules consisting of two distinct, spatially separate gas components: a central, isothermal region surrounded by a negative-index, polytropic envelope. The clouds are supported against their own self-gravity by a combination of thermal, mean magnetic, and turbulent wave pressure. The latter two are included by allowing for locally adiabatic, non-isentropic pressure components. Such models are meant to represent, in a schematic manner, the velocity and density structure of cores and globules, as inferred from molecular line and dust continuum observations. In addition, our picture reflects the theoretical expectation that MHD wave motions, which are important at scales $\gtrsim 0.1$ pc in typical low-mass star-forming regions, are damped at smaller scales, giving rise to a finite-sized, thermally-dominated core region. We show that if the pressure components are isentropic, then the pressure drop from the center to the edge of the composite polytropes we consider is limited to 197, the square of the value for the Bonnor-Ebert sphere. If the pressure components are non-isentropic, it is possible to have arbitrarily large pressure drops, in agreement with the results of McKee & Holliman (1999). However, we find that even for non-isentropic pressure components, the ratio of the *mean* to surface pressure in the composite polytropes we consider is less than 4. We show by explicit construction that it is possible to have dense cores comparable to the Jeans mass embedded in stable clouds of much larger mass. In a subsequent paper, we show that composite polytropes on the verge of gravitational instability can reproduce the observed velocity and density structure of cores and globules under a variety of physical conditions.

Subject headings: ISM: clouds — ISM: globules — ISM: structure — Stars: formation

1. INTRODUCTION

Observations of cold, dense molecular clouds in the interstellar medium present a unique challenge to theorists. Isolated Bok globules and dense molecular cores in molecular cloud complexes, in particular, are definitive testbeds for theories of molecular cloud structure and low-mass star formation. As “the simplest unit structures in the dense interstellar medium” (Dickman & Clemens 1983), an adequate description of these objects should contribute significantly to our understanding of the molecular component of the Galaxy as a whole.

1.1. *Observed Properties of Dense Cores and Bok Globules*

Dense cores are compact regions within molecular clouds whose number density exceeds about 10^4 cm⁻³. The connection of these regions to star formation in the complexes has been explored in some detail (Loren 1989; Onishi et al 1998); in many cases there is close spatial agreement between young stars and cores (Beichman et al 1986). In fact, IRAS sources have been detected in approximately half of the known (~ 100) nearby cores (Benson & Myers 1989). The relatively isolated cores in Taurus, which have been extensively surveyed in NH₃ (Myers & Benson 1983; Benson & Myers 1989), have sizes on the order of 0.1 pc, masses $\sim 1 - 10 M_{\odot}$, kinetic temperatures ~ 10 K, and NH₃ linewidths ~ 0.3 km s⁻¹. The narrow linewidths suggest that these objects are relatively quiescent;

thermal motions are responsible for at least half of the observed line broadening. This is in contrast to the well-known increase of nonthermal linewidth with size scale in the regions immediately surrounding the ammonia cores (Fuller & Myers 1992; Goodman et al 1998). The properties of cores in more crowded regions, such as Ophiuchus and Orion, differ from those in Taurus mainly insofar as they tend to be more massive and compact, and have higher temperatures and linewidths (Caselli & Myers 1995; Motte, André, & Neri 1998).

A catalog of 248 optically selected Bok globules was compiled by Clemens & Barvainis (1988). A comparison of these objects with the Benson & Myers (1989) sample of dense cores in molecular cloud complexes reveals that the two populations are quite similar, with a trend toward higher masses and densities (by about a factor of two) in the dense cores (Bourke et al. 1995). Associated IRAS point sources have been detected in about one-quarter of the Bok globules, down to a detection limit of $0.7 M_{\odot}$ (Yun & Clemens 1990). The degree of similarity is perhaps surprising, given the different environments in which the two types of object reside. For example, the two populations should differ with respect to their exposure to the interstellar radiation field. Whereas cores in complexes are often shielded from such radiation by their parent clouds (Benson & Myers 1989; Onishi et al 1996), photoelectric heating from the interstellar radiation field is expected to produce an outward temperature gradient in Bok globules lacking embed-

¹Present address: Department of Physics and Astronomy, University of Western Ontario, London, ON N6A 3K7

²Email: curry@astro.uwo.ca

ded young stars (Boland & de Jong 1984). This effect has been observed in dark clouds and cores in close proximity to star-forming regions (Young et al 1982; Bachiller, Guilloteau, & Kahane 1987), but direct evidence for isolated Bok globules is more scarce. According to Clemens, Yun, & Heyer (1991), the spectral energy distributions of globules in the Clemens & Barvainis sample preclude single-temperature models for all objects. On the other hand, molecular line observations of objects in the same sample display remarkably uniform temperatures over their projected areas (Lemme et al 1996). The latter might be explained, however, by the fact that the dense molecular tracers used in such studies do not sample the outer, more exposed regions of the globules.

1.2. Virial Parameters: Implications for Stability

A key question relating to cores and Bok globules is: how near are they to gravitational collapse? A stable interstellar cloud need not be highly centrally condensed and self-gravitating; it can also be nearly uniform and confined by an external pressure. In an analysis of clump data³ from several active star-forming regions, Bertoldi & McKee (1992) noted a correlation between the “observed virial parameter” for a clump, $\alpha = 5\bar{R}\langle\sigma^2\rangle/GM$, and the clump mass, M . Here, $\langle\sigma^2\rangle$ is the mean square velocity along the line of sight and \bar{R} an average cloud radius, both determined from intensity contours in the $J = 1 - 0$ line of ^{13}CO .⁴ Stable clumps with $\alpha \gg 1$, they argued, are likely to be confined by the pressure of the external medium, and not very centrally concentrated, while those with $\alpha \sim 1$ would be expected to be strongly condensed and self-gravitating (no clumps with $\alpha \ll 1$ were observed; such clumps are unstable and would collapse unless supported by a strong magnetic field). The authors’ analysis revealed that only the most massive clumps ($\gtrsim 100 M_{\odot}$) in the complexes had $\alpha \sim 1$, and thus that the majority of the clumps seen were likely to be pressure-confined. For example, representative values for a $\sim 10 M_{\odot}$ clump in Ophiuchus from Loren (1989) are $\sigma \simeq 0.46 \text{ km s}^{-1}$ and $\bar{R} \simeq 0.43 \text{ pc}$, implying $\alpha \simeq 10.5$.

It is important to emphasize that estimates of α from molecular line studies are highly dependent on the observed molecule. Dense molecular tracers, such as NH_3 and CS , are generally only excited in small regions where the mean density of hydrogen exceeds $\sim 10^4 \text{ cm}^{-3}$. The mean density of the Ophiuchus ^{13}CO clumps, on the other hand, is only $\sim 3 \times 10^3 \text{ cm}^{-3}$. It is therefore desirable to recalculate α for these denser molecular tracers, in order to ensure that one is truly probing the densest gas. For this purpose, we turn to the NH_3 study of dense cores by Myers & Benson (1983). Mean values from their sample are: $\bar{\sigma} \simeq 0.23 \text{ km s}^{-1}$, $\bar{R} \simeq 0.06 \text{ pc}$, and $M \simeq 4.1 M_{\odot}$. These yield $\alpha \simeq 0.9$, indicating that the cores in their sample, which are of very low mass compared to those in the ^{13}CO studies, are nevertheless nearer to a state of marginal stability. Further support is provided by dust continuum studies in Ophiuchus, which also give $\alpha \sim 1$ for cores of this size and smaller (Motte et al 1998).

In this paper, we adopt the view that both low- and high-mass cores that have been detected in ammonia and other

dense molecular tracers (e.g. C^{18}O and CS) are near a state of marginal stability, or, as we shall refer to it, near the *critical point*. The latter is more precisely defined as the unique state such that, upon suffering a small perturbation at its surface, the cloud must collapse. These cores may themselves be embedded in molecular gas that is gravitationally bound to the core; however, we assume that this external gas acts primarily to set the pressure at the surface of the core, not to determine the cloud stability.

1.3. The Initial Conditions for Star Formation

1.3.1. Pre-Protostellar Cores

The high percentage of dense cores and Bok globules with embedded IRAS point sources can, in principle, put restrictions on theories of star formation. Furthermore, the roughly equal samples of “starless” cores and Bok globules should place constraints on the initial conditions for protostellar collapse, assuming that these clouds still have a reasonable chance of forming stars (§1.2). Hence the recent usage of the term “pre-protostellar core” to denote these objects (Ward-Thompson et al 1994; André, Ward-Thompson, & Motte 1996). We shall henceforth refer to both starless dense cores found within GMCs and starless Bok globules by the latter term, for brevity abbreviated to PPC. In the quasi-static picture of low-mass star formation, PPCs evolve from low density and possibly low mass along a near-equilibrium sequence of denser, possibly more massive states, until a state of marginal stability is reached. This evolution may be achieved in a number of ways: ambipolar diffusion is likely to play a key role, and possibly ongoing accretion from the surrounding medium (Mestel & Spitzer 1956; Boland & deJong 1984; Bonnell, Bate, & Price 1996). As defined, PPCs generally only form one or at most a small group of stars.

Historically, theories of cloud equilibria have been intimately connected with calculations of gravitational collapse, inasmuch as the former fill the important role of initial conditions for the latter. Models with singular density profiles are often adopted for computational simplicity. In particular, the singular isothermal sphere (hereafter SIS), which has a static density structure given by $\rho(r) \propto r^{-2}$, has been extensively studied. This model is unstable to collapse, and has a corresponding time-dependent solution first studied by Shu (1977).

As a model for PPCs, there are three principal caveats to the SIS, two of which stem directly from observation. The first is the existence of a nonthermal component of the molecular linewidth in PPCs. The nonthermal line width increases with size scale as $r^{0.5}$ in low-mass cores and as $r^{0.2}$ in high-mass cores (Caselli & Myers 1995). As mentioned in §1.1 above, thermal motions prevail within $\sim 0.1 \text{ pc}$ of the intensity maximum; but even along the line of sight toward the intensity maximum, a finite nonthermal component is detected (Goodman et al 1998). Second, most objects that have been mapped with sufficient resolution exhibit non-singular—indeed, nearly flat—column density profiles as one approaches the intensity maximum. This is true of both stable Bok globules (Dickman & Clemens 1983; Turner, Xu, & Rickard 1992; Lehtinen et

³We shall follow the terminology of Williams, Blitz, & McKee (1999) in describing the structure of molecular clouds. “Clumps” are coherent regions in $l-b-v$ space, generally identified from spectral line maps of molecular emission. Star-forming clumps are the massive clumps out of which stellar clusters form; cores (sometimes referred to as “dense cores”) are the regions out of which individual stars or stellar systems form. The clumps studied by Bertoldi & McKee were identified based on ^{13}CO line maps, whereas dense cores in low-mass star-forming regions are generally within star-forming clumps and are identified from their NH_3 emission.

⁴Assigning a “radius” to a non-spherical clump or core is common practice. The authors showed that, if α is interpreted as an average over all orientations of an ellipsoidal cloud, then this approximation is likely to be in error by no more than 30%.

al 1995) and dense cores (Gaida, Ungerechts, & Winnewisser 1984) mapped in molecular lines, as well as PPCs mapped in sub-mm dust continuum (Casali 1986; Ward-Thompson et al 1994; Motte et al 1998). In contrast, radial profiles of cores *with* embedded stars lack such an extended, flat inner region, and tend to be more compact than PPCs (Motte et al 1998).

An additional, theoretical, argument against the SIS model is that there is no known way for a cloud to evolve to a *static* SIS, since isothermal spheres are unstable to gravitational collapse for center-to-surface density ratios greater than 14 (Ebert 1955; Bonnor 1956). Models of the collapse of isothermal clouds (Hunter 1977; Foster & Chevalier 1993) and of magnetized clouds (Safier, McKee, & Stahler 1997) show that a $1/r^2$ structure does develop during the collapse, but it is not static; as a result, the accretion rate at early times is greater than that predicted by the SIS model. However, at late times, both solutions behave similarly to the SIS.

These considerations argue both against a singular density profile toward the centers of PPCs, and against the existence of a purely thermal region filling most of the PPC. On these grounds, we conclude that PPCs *as a whole* are unlikely to bear any close relation to (singular or non-singular) isothermal spheres.

1.4. Previous Models of Self-Gravitating Cloud Equilibria

Any complete model of a molecular cloud must include a detailed treatment of thermal balance throughout the gas, which entails a full description of the physical and chemical properties at every point. While progress has been made along these lines (de Jong, Dalgarno, & Boland 1980; Falgarone & Puget 1985), polytropic models, which postulate a power-law relation between pressure and density at each point,

$$P = K_p \rho^{\gamma_p} = K_p \rho^{1 + \frac{1}{n}}, \quad (1)$$

are often adopted as a simplifying assumption. Here, K_p is constant and γ_p and n are different versions of the polytropic index. Yet, spherical, non-singular, polytropic models of dense cores and Bok globules have met with only limited success. Somewhat surprisingly, the dominant problem lies not with details of chemistry, but rather in simultaneously reproducing the bulk properties—mass, radius, and density contrast—of the objects.

Positive-index polytropes ($n > 0$, $\gamma_p > 1$) cannot account for the observed variation of line width with radius in molecular clouds since their temperatures decrease with radius (Shu et al 1972). Gas temperatures in cores and globules are found to be either uniform, at $T \simeq 10$ K (perhaps a factor of 2–3 higher in more massive objects and in regions with recent nearby star formation), or outwardly increasing (Bachiller et al 1987). Furthermore, on nearly all spatial scales, the nonthermal linewidth increases with size (Larson 1981). Negative-index polytropes ($n < -1$, $0 < \gamma_p < 1$; hereafter, NIPs), which have a temperature $T \propto P/\rho \propto \rho^{1/n}$ that increases with linear scale, can qualitatively reproduce this behavior if the polytropic temperature is taken to represent the *total* velocity dispersion (Maloney 1988); i.e., $T_{NIP}(r) \propto P(r)/\rho(r) \propto \sigma^2(r)$. The limiting case of the NIP as $\gamma_p \rightarrow 0$ is the “logatropes”, introduced by Lizano & Shu (1989) as a phenomenological model for turbulent pressure and studied further by McLaughlin & Pudritz (1996) and Gehman et al (1996).

Molecular clouds and Bok globules are supported by several different pressure components—in addition to the thermal and turbulent pressures discussed above, there is also the static

magnetic field. Mouschovias (1976) and Tomisaka, Ikeuchi, & Nakamura (1988) developed models of axisymmetric clouds supported by static magnetic fields and isothermal gas. Lizano and Shu (1989) extended these calculations to include turbulent pressure, modeled as a logatropes. More recently, McKee & Holliman (1999; hereafter MH) developed *multi-pressure polytrope* models for clouds, in which each of the important pressure components is represented by an appropriate polytrope. Comparison of these models with observations was carried out by Holliman (1995). A phenomenological alternative to multi-pressure polytropes is the “TNT” model developed by Myers & Fuller (1992) and Caselli & Myers (1995). In this model, the density is assumed to be the sum of two terms,

$$n \propto \left(\frac{r_0}{r}\right)^2 + \left(\frac{r_0}{r}\right)^p,$$

where the first represents the effect of thermal pressure and the second the effect of nonthermal pressure. By inserting this expression into the equation of hydrostatic equilibrium, it is possible to infer both the density at r_0 and the variation of the line width with r ; reasonably good fits are obtained for most cores by an appropriate choice of the parameters r_0 and p .

Fits of the envelopes of globules in the Clemens & Barvainis sample to a volume density law of the form $n(r) \propto r^{-k_p}$ indicate a rather narrow range: $1 \lesssim k_p \lesssim 2$ (Yun & Clemens 1991). This further supports the use of NIPs, whose behavior asymptotically approaches a power law with precisely the same range of indices. [The singular polytropic sphere has $n(r) \propto r^{-2/(2-\gamma_p)} = r^{-2n/(n-1)}$.] Similar fits to dense core data produce the same range of k_p (Cernicharo, Bachiller, & Duvert 1985; Bachiller et al 1987; Stüwe 1990). The use of NIPs in the thermal modeling of molecular clouds has been validated by de Jong et al (1980), Boland & de Jong (1984), and Falgarone & Puget (1985), each of whom attempted to determine the equation of state relevant to dense molecular gas using detailed thermal and chemical balance calculations. While the representation of turbulence as a spatially varying isotropic pressure is clearly simplistic, Alfvén waves, a significant contributor to MHD turbulence, have a polytropic index $\gamma_p = 1/2$, corresponding to $n = -2$ (Walén 1944; McKee & Zweibel 1995).

Non-singular NIPs that are truncated by a medium of constant pressure have well-defined stability properties. In keeping with the above discussion of virial equilibrium, it is of interest to compare the theoretical properties of critically stable NIPs with the observed masses, radii, and density contrasts of PPCs. Under the usual assumptions that the NIP is isentropic (see §2.1), the mass, radius, and density contrast cannot exceed the values (Viala & Horedt 1974),

$$R_{BE} = 0.485 \frac{c_s^2}{(GP_s)^{1/2}} \quad M_{BE} = 1.18 \frac{c_s^4}{(G^3 P_s)^{1/2}}, \quad \left(\frac{\rho_c}{\rho_s}\right)_{BE} = 14.04,$$

where M_{BE} , R_{BE} , and $(\rho_c/\rho_s)_{BE}$ are the mass, radius and density contrast of the critically stable, bounded isothermal sphere, also known as the Bonnor-Ebert sphere (Ebert 1955; Bonnor 1956). That is, the Bonnor-Ebert sphere (which has $n = \pm\infty$, $\gamma_p = 1$) sets the upper limits of the physical parameters for any NIP, provided that the sound speed, $c \equiv (P/\rho)^{1/2}$, in the isothermal sphere is the same as the *surface* value, c_s , in the NIP. The same limits apply if c_s is replaced by the rms sound speed in the cloud, $\langle c^2 \rangle^{1/2}$, which is often more easily observed than c_s (MH). The fact that $\alpha \sim 1$ for observed PPCs ensures

that their masses and radii are in reasonable accord with the above, provided that c includes both thermal and nonthermal motions. However, the inferred density contrast between the intensity peak of many cores and the boundaries of their surrounding clumps (as determined from ^{13}CO) is typically $\gtrsim 30$ (Stutzki & Guesten 1990; Williams, Blitz, & Stark 1995; André et al 1996), which significantly exceeds $(\rho_c/\rho_s)_{BE} = 14.04$. The problem may be even more pronounced for Bok globules, which are expected to have a lower boundary pressure than cores since they are not embedded in GMCs. As stated succinctly by Hasegawa (1988), who attempted to model the Bok globules L134 and L183, "...a single hydrostatic gas sphere cannot explain the high density contrast between the environment and the center of globules."

Attempts have been made to elude this difficulty. In their model of a quiescent Bok globule, Dickman & Clemens (1983) proposed a new stability criterion for NIPs; namely, that the central temperature, not the entropy, remains constant during a perturbation (see Appendix). This criterion was later adopted by Maloney (1988), who explicitly showed that it renders all bounded NIPs unconditionally stable. Of course, this removes the upper bound on the density contrast given above, allowing it to be fit to observations. Predictably, however, this can result in an overestimate of the mass, radius, and visual extinction of the object (Hasegawa 1988; Turner et al 1992). An important exacerbating factor in the modelling difficulties faced by both Dickman & Clemens and Hasegawa was their assumption that the total boundary pressure was equal to the thermal pressure ($P_{\text{th}} \lesssim 3700 \text{ K cm}^{-3}$) *only*. In contrast, current estimates including the interstellar magnetic field (but not cosmic rays, which pervade both the cloud and the ambient medium) give $P \simeq 2 \times 10^4 \text{ K cm}^{-3}$ (Boulares & Cox 1990). While this lessens somewhat the discrepancies they uncovered, it does not solve the problem. Nor does it change the fact that NIPs of any radius are unable to fit the detailed shape of the line width–size relation (Paper II).

Implicit in the stability analyses described so far is the assumption that the gas sphere responds *isentropically*, i.e. with spatially and temporally constant entropy, to perturbations applied at its surface. While this is appropriate for an isothermal gas alone, observations suggest a more complex situation, in which several distinct pressure components—primarily thermal, magnetic, and turbulent—coexist in the gas (Myers & Goodman 1988). As shown recently by MH, this necessitates a *non-isentropic* description of cloud structure (the significance of this will be discussed in §2 below). Non-isentropic polytropes that accurately reflect the relative pressures of these distinct components tend to be more stable than their isentropic counterparts. This improved treatment obviates the perceived need for the ad hoc, constant central-temperature restriction introduced by the above authors (see Appendix).

1.5. Motivation and Evidence for Core-Envelope Structure

In this paper, we construct a model for PPCs that explicitly reflects their observed velocity structure; i.e., thermal and subsonic nonthermal motions on small scales ($\lesssim 0.1 \text{ pc}$), and supersonic nonthermal motions on larger scales. Theoretically, the transition between the two regimes is believed to occur via the damping of Alfvén waves in regions of low ionization; i.e. near the density maximum where the optical depth to incoming FUV photons is largest. The critical wavelength for damping is of order 0.1 pc , under typical PPC conditions (§2.2). This suggests, in the apt description of Goodman et al. (1998), a view of

PPCs as “islands of calm in a turbulent sea.”

Another theoretical argument for such a division comes from the theory of magnetized molecular clouds in the absence of wave motions. Central to the quasi-static picture is the notion of a magnetically-supported cloud, slowly contracting via ambipolar diffusion (Mouschovias 1991). Over time, magnetic support in the central region decreases as the mass and density increase there, while in the envelope, little changes. This leads naturally to a division between core and envelope, in that the latter remains “magnetically subcritical,” while the core becomes “magnetically supercritical” (McKee et al 1993). Eventually, the core alone collapses, leaving behind the magnetically subcritical envelope that accretes more slowly (Safier et al 1997). Inclusion of the effects of hydromagnetic waves should moderate the inward flow of mass via ambipolar diffusion, but the decay of the waves in the central region should allow it to operate as predicted, preserving—and perhaps enhancing—the distinction between core and envelope (see also Mouschovias 1991).

Studies of the thermal structure of clouds exposed to the interstellar radiation field also suggest a core-envelope structure. Falgarone & Puget (1985) studied the effect of external infrared and UV radiation on thermally-supported self-gravitating condensations of gas and dust. For the conditions they assumed, they found equilibria featuring isothermal, molecular cores (of typical radius 0.1 pc and mass $2 M_{\odot}$) surrounded by warmer and more diffuse, partially atomic, envelopes (with $r \sim 1 \text{ pc}$, $M \sim 10 M_{\odot}$, depending on the UV field intensity and external pressure). More recently, detailed numerical calculations by Nelson & Langer (1997) demonstrated that the thermal evolution of a $100 - 400 M_{\odot}$, uniform density cloud subjected to the interstellar radiation field leads to a core-envelope structure, in which the core region has roughly the same properties as those observed for PPCs in C^{18}O , while containing only one-fifth of the total mass. Elmegreen (1989) calculated the relative mass and radius fractions of molecular cores to atomic envelopes for spherical polytropes exposed to the interstellar radiation field. While this molecular/atomic core–envelope structure is generally not relevant to PPCs, which are shielded by the ambient molecular gas, it may be relevant to the more massive Bok globules, which have bulk properties quite similar to those predicted by the models of Nelson & Langer (1997), except for the large nonthermal linewidths in their envelopes.

On the observational side, Bachiller & Cernicharo (1984) noted marked differences in the density and velocity structure of the large dark cloud B1 depending on the molecular tracer used, prompting them to divide the cloud into an NH_3 core ($r \lesssim 0.3 \text{ pc}$, $M \lesssim 60 M_{\odot}$), a C^{18}O and ^{13}CO envelope ($r \lesssim 1 \text{ pc}$, $M \lesssim 350 M_{\odot}$), and a ^{12}CO halo ($r \sim 2 \text{ pc}$, $M \sim 400 M_{\odot}$). Interestingly, despite these differences, the three regions showed negligible variations in kinetic temperature ($T = 12 \pm 2 \text{ K}$). While this layering could simply reflect the density threshold at which different molecular species are excited, a later study of similar clouds in the Taurus-Auriga-Perseus complex using dust extinctions to derive H_2 column densities found similar results (Cernicharo et al 1985). On smaller scales, Fuller (1989) proposed the same division on the basis of higher-resolution NH_3 and C^{18}O observations.

As a particular example of a cloud one might keep in mind for our models, consider R65, a well-studied, starless clump in the $\rho \text{ Oph}$ complex (Loren 1989). ^{13}CO maps of this clump give the following estimates: $T \approx 20 \text{ K}$, FWHM size $\approx 0.77 \times 0.44$

pc, $\bar{n}_{H_2} \approx 3.5 \times 10^3 \text{ cm}^{-3}$, $\sigma \approx 0.39 \text{ km s}^{-1}$, and $M \approx 21 M_\odot$; no IRAS sources were detected within the FWHM contour. Note that we have assumed a H_2 to ^{13}CO abundance ratio of 4.8×10^5 , in accord with the downward revision in Loren's original estimate by Bertoldi & McKee (1992). Using these values, and taking for R one-half of the geometric mean of the cloud dimensions, one finds $\alpha \approx 2.4$. The dense core of R65, L1689B, has been detected in C^{18}O , NH_3 (Benson & Myers 1989) and, more recently, 1.3 mm dust continuum (André et al 1996). The latter study gives: $T \approx 18 \text{ K}$, FWHM geometric mean radius $\approx 0.046 \text{ pc}$, $\bar{n}_{H_2} \approx 4.1 \times 10^4 \text{ cm}^{-3}$, and $M \approx 1 M_\odot$. According to André et al, the derived density contrast between the intensity peak of L1689B and the edge of R65 is $\gtrsim 30$, a figure much higher than simple equilibrium NIP models can accommodate, even at their critical states (i.e. $\rho_c/\rho_s \leq 14.04$).

In §2, we develop the theory of polytropes with core-envelope structures in detail, including an analysis of their stability. After reviewing the properties of single-component polytropes in §3, we examine the physical properties of composite polytropes in §4. Some of the broader implications of these properties for star formation in PPCs are mentioned in §5. In a subsequent paper, we compare the models to available observations.

2. COMPOSITE POLYTROPES: GENERAL THEORY

2.1. Locally Adiabatic Pressure Components

Polytropic models have long been used to model molecular clouds. The discussion of the data on molecular cloud cores and Bok globules above suggests that two generalizations of the standard polytropic theory are needed in order to successfully model these objects: First, as mentioned above, it is necessary to include several different pressure components, each with pressure $P_j(r)$, so that the total pressure is $P = \sum P_j$. If $\gamma_{p,j}$ is the polytropic index for the j th pressure component, then the polytropic index for the resulting multi-pressure polytrope is given by (MH)

$$\gamma_p \equiv \frac{d \ln P}{d \ln \rho} = \sum_{j=1}^N \left(\frac{P_j}{P} \right) \gamma_{p,j}, \quad (2)$$

where N is the number of distinct pressure components. To simplify the analysis, we make the approximation in this paper that the spatially varying polytropic index $\gamma_p(r)$ can be replaced by a suitable average, $\bar{\gamma}_p$.

Second, it is necessary to consider two (or more) spatially distinct polytropic regions, each with its own polytropic index—a *composite polytrope*. For a core and an envelope, we write

$$P_{\text{core}} = K_{\text{core}} \rho^{\bar{\gamma}_{p,\text{core}}} \quad P_{\text{env}} = K_{\text{env}} \rho^{\bar{\gamma}_{p,\text{env}}},$$

where K_{core} and K_{env} are constants. Composite polytropes have found wide application in stellar structure: Milne (1930, 1932) constructed such models for stars with degenerate cores. Henrich & Chandrasekhar (1941) considered models of a star with an isothermal core and an $n = 3$ (radiative) envelope, while Schönberg & Chandrasekhar (1942) investigated the effect of compositional gradients in such models. The radial stability of a composite polytrope with an isothermal core and an $n = 3/2$ ($\gamma_p = 5/3$) envelope was studied by Yabushita (1975) in the context of neutron stars. More recently, Beech (1988) constructed

an analytic model for low-mass stars, joining an approximate solution for a $n = 3$ ($\gamma_p = 4/3$) polytrope onto a $n = 1$ ($\gamma_p = 2$) envelope.

The specification of $\bar{\gamma}_p$ in each of the two regions suffices for the determination of an entire equilibrium sequence; e.g., the total mass as a function of central density. In order to decide the issue of stability for members of that sequence, however, one needs to know the response of each pressure component to small perturbations. We shall assume in this work that: (1) the perturbations are adiabatic, and; (2) for each component, the time scale for internal heat transfer—a direct consequence of the perturbation—is long compared to the dynamical time scale. Following MH, we refer to the latter as “locally adiabatic” pressure components⁵. Such components satisfy the usual adiabatic relation (Ledoux & Walraven 1958),

$$\delta \ln P_j = \gamma_j \delta \ln \rho,$$

where the different pressure components are assumed to be thermally insulated from each other. The adiabatic indices γ_j , then, describe *temporal* variations of the pressure components, while the polytropic indices, $\gamma_{p,j}$, describe *spatial* variations. For locally adiabatic polytropes, MH show that the overall adiabatic index is

$$\gamma \equiv \frac{\delta \ln P}{\delta \ln \rho} = \sum_{j=1}^N \left(\frac{P_j}{P} \right) \gamma_j. \quad (3)$$

For the purposes of this discussion, we shall assume that, as in the case of the polytropic indexes, this spatially varying adiabatic index can be approximated by a mean adiabatic index in each region, $\bar{\gamma}$. Calculations using multi-pressure polytropes (MH) do not suggest a simple prescription for determining $\bar{\gamma}_p$ or $\bar{\gamma}$ from the properties of the constituent polytropes. However, these calculations do indicate that $\bar{\gamma}_p$ and $\bar{\gamma}$ are weighted means in the sense that if there are two pressure components with adiabatic indexes γ_1 and γ_2 , for example, then $\gamma_1 < \bar{\gamma} < \gamma_2$. In Paper II we shall infer values of $\bar{\gamma}_p$ and $\bar{\gamma}$ from observations.

When $\bar{\gamma}_p = \bar{\gamma}$ in a region, the gas is isentropic there (i.e., it has a constant specific entropy), and as a result no internal heat transfer is required to maintain the polytropic structure after a perturbation. Most studies of polytropic models for interstellar clouds have assumed that the clouds are isentropic. More generally, however, $\bar{\gamma}_p \neq \bar{\gamma}$. For example, small-amplitude, undamped Alfvén waves have $\gamma_{p,w} = 1/2$ and $\gamma_w = 3/2$ (McKee & Zweibel 1995). Note that when $\gamma < \gamma_p$, polytropic spheres are convectively unstable according to the Schwarzschild criterion (Cowling 1941); none of the known pressure components are in this regime, however. For the pressure components in molecular clouds, we have $\gamma_{\text{th}} = \gamma_{p,\text{th}}$ for the isothermal gas; $\gamma_B \geq \gamma_{p,B}$ for the magnetic field in order that the cloud be stable against the interchange instability; and, as we have just seen, $\gamma_w > \gamma_{p,w}$ for the Alfvén waves. Since each pressure component has $\gamma \geq \gamma_p$, we expect $\bar{\gamma} \geq \bar{\gamma}_p$ in each part of a composite polytrope model for molecular clouds. This is significant, since non-isentropic polytropes are *more* stable than their isentropic counterparts (MH). This is essentially due to the fact that as $\bar{\gamma}$ approaches $4/3$, single-component polytropes are unconditionally stable (Ledoux & Walraven 1958).

⁵MH also consider the case in which the timescale for internal heat transfer is short compared to the dynamical timescale; they term such components “globally adiabatic.”

2.2. Core Properties

All available evidence suggests that the dense, thermally-dominated core of a PPC is an unusually quiescent region, in comparison to its surroundings. We presume, as have others, that there is a scale above which the cloud is supported against its own weight primarily by a mean magnetic field and MHD waves (Shu, Adams, & Lizano 1987; McKee et al 1993); for typical low-mass star-forming regions in Galactic molecular clouds, this length scale is about 0.1 pc. In the core, however, the observed near-thermal velocity linewidths suggest that the waves important for maintaining equilibrium on large scales are damped at smaller scales; specific damping mechanisms for MHD waves were discussed by Zweibel & Josafatsson (1983). The cutoff wavelength for damping along the direction of the field has been estimated as (Kulsrud & Pearce 1969)

$$\lambda_{\text{cut}} = 0.13 \text{ pc} \left(\frac{B}{20 \mu\text{G}} \right) \left(\frac{n_{\text{H}_2}}{10^3 \text{ cm}^{-3}} \right)^{-1} \left(\frac{\zeta_{\text{CR}}}{10^{-17} \text{ s}^{-1}} \right)^{-1/2}, \quad (4)$$

where B and n_{H_2} are characteristic values of the magnetic field strength and H_2 density in the relevant region, and ζ_{CR} is the cosmic-ray ionization rate. We have assumed the standard balance between ionization and recombination in order to compute the coefficient (McKee et al 1993). However, ζ_{CR} can range between $10^{-18} \lesssim \zeta_{\text{CR}} \lesssim 10^{-16}$ depending on the degree of shielding (Caselli et al 1998), meaning that λ_{cut} is uncertain by as much as a factor of 3 in either direction. Nevertheless, equation (4) suggests an important constraint on the models; i.e. that the thermally dominated core region should have a radius $r_{\text{core}} \simeq \lambda_{\text{cut}}/2$.

We now turn to the polytropic and adiabatic indices. By construction, $\gamma_{p,\text{th}} = \gamma_{\text{th}} = 1$. The value of $\gamma_{p,B}$ is somewhat more uncertain; it depends both on the degree of isotropy in the contraction of the cloud from a more uniform initial state, and on the amount of ambipolar diffusion that has taken place. For a PPC formed by compressing a uniform density cloud under strict flux conservation (i.e. no ambipolar diffusion), $\gamma_{p,B} = 4/3$, while for a PPC of ‘‘infinite age’’ (i.e. maximal ambipolar diffusion), $\gamma_{p,B} = 0$. As an intermediate value, we shall assume $\gamma_{p,B} = 1$ in the core of our composite polytrope, indicating a moderate amount of ambipolar diffusion. Since this is identical to the value of γ_p for the gas pressure, the other pressure component in the core, we adopt $\bar{\gamma}_{p,\text{core}} = 1$; thus, the isothermal solution can be used for the core. In a subsequent paper, we shall use observations to estimate a range of likely values for $\bar{\gamma}_{p,\text{core}}$, and show that this too is consistent with the use of the isothermal approximation. Since the redistribution of flux is negligible on the time scale of the perturbation, we take $\gamma_B = 4/3$, appropriate for adiabatic, flux-conserving compression. We expect the adiabatic index for the core to have a value intermediate between that of the thermal gas and the magnetic field: $1 \lesssim \bar{\gamma}_{\text{core}} \lesssim 4/3$.

2.3. Envelope Properties

The observed increase of nonthermal linewidth with size to supersonic values in molecular clouds strongly suggests the presence of MHD turbulence at scales larger than about 0.1 pc. We therefore include a third, Alfvén-wave pressure component, \bar{P}_w , in the total mean pressure of the envelope.

The assumption of a polytropic relation for Alfvén waves was examined by McKee & Zweibel (1995). They showed that as long as the waves are linear in amplitude, undamped,

and of wavelengths shorter than variations in the background density, they exert an isotropic pressure obeying $P \propto \rho^{\gamma_p}$ with $\gamma_p = 1/2$ (this relation was originally derived by Walén 1944). Further, the adiabatic index of such waves is $\gamma_w = 3/2$. Now, were Alfvén waves treated as a locally adiabatic pressure component, they would be unconditionally stable, since $\gamma_w > 4/3$. However, as argued by MH, undamped Alfvén waves are more likely to behave as a globally adiabatic pressure component, since wave energy tends to flow from high to low density regions in a centrally-concentrated cloud. These authors demonstrated that single-component, globally adiabatic spheres are generally less stable than their locally adiabatic cousins. In particular, a critically stable cloud with $\gamma_p = 1/2$ and $\gamma_w = 3/2$ has a finite center-to-surface pressure contrast of 4.15, and a density contrast of 17.26.

In our description, in which Alfvén waves are treated in an averaged sense, we make the approximation that the waves, like the mean magnetic field, are locally adiabatic. As shown by MH, the location of the critical point for a multi-pressure polytrope including Alfvén waves is the same as that for a similar multi-pressure polytrope in which the Alfvén waves are replaced by a locally adiabatic pressure component with $\gamma_{p,j} = 1/2$ and with a suitable value of γ_j . For a cloud supported entirely by Alfvén waves, the value of γ for the equivalent locally adiabatic component is $\gamma_{w,\text{eq}} = 0.6056$. However, as other pressure components become important, the value of $\gamma_{w,\text{eq}}$ increases, which complicates the choice a suitable value for $\bar{\gamma}$. In any case, since $\bar{\gamma}$ is some weighted mean of the γ_j ’s of the individual components, we expect $\bar{\gamma} < 4/3$.

We now proceed to the actual construction of composite polytropes, starting with the illustrative example of the composite isothermal sphere. Note that in what follows, we omit the overline indicating the averaged character of γ_p and γ ; for the theory, it matters only that they are constants.

2.4. Isothermal Cores and Envelopes

In order to gain a feel for composite equilibria, we begin with the illustrative example of the composite isothermal sphere. Consider a core of isothermal gas at temperature T_{core} surrounded by an isothermal envelope at temperature $T_{\text{env}} > T_{\text{core}}$. Let $c_{\text{core, env}}$ denote the constant isothermal sound speed in the core and envelope, respectively. Define the jump in conditions at the interface by

$$\tau_i \equiv \left(\frac{c_{\text{env}}}{c_{\text{core}}} \right)^2 = \frac{T_{\text{env}}}{T_{\text{core}}} > 1, \quad (5)$$

where in the second step we have assumed both regions to be of the same composition.

Introducing the customary dimensionless variables ξ and $\psi(\xi)$ (Chandrasekhar 1939), the density, radius, and mass within the core are given by

$$\rho = \rho_c \exp(-\psi), \quad (6)$$

$$r = r_{\text{ch}} \xi \equiv \frac{c_{\text{core}}}{(4\pi G \rho_c)^{1/2}} \xi, \quad (7)$$

$$M(r) = 4\pi \rho_c r_{\text{ch}}^3 \xi^2 \frac{d\psi}{d\xi}, \quad (8)$$

where ρ_c is the density at the center ($r = 0$) and r_{ch} is a characteristic radius proportional to the Jeans length in the core. In the interest of notational simplicity, it is desirable to retain ξ and ψ

in the envelope as well as in the core. In the envelope then,

$$\begin{aligned}\rho &= \rho_e \exp(-\psi), \\ r &= r_{\text{ch}} \xi \equiv \frac{c_{\text{env}}}{(4\pi G \rho_e)^{1/2}} \xi, \\ M(r) &= 4\pi \rho_e r_{\text{ch}}^3 \xi^2 \frac{d\psi}{d\xi},\end{aligned}\quad (9)$$

where ρ_e is an undetermined constant.

At the interface of core and envelope, the radius, pressure, and mass must be continuous (but *not* the density; the present class of models differs from composite *stellar* models in precisely this sense). The above expressions therefore give

$$\begin{aligned}c_{\text{core}}^2 \rho_c \exp(-\psi_-) &= c_{\text{env}}^2 \rho_e \exp(-\psi_+), \\ c_{\text{core}} \rho_c^{-1/2} &= c_{\text{env}} \rho_e^{-1/2}, \\ c_{\text{core}}^3 \rho_c^{-1/2} \psi'_- &= c_{\text{env}}^3 \rho_e^{-1/2} \psi'_+, \end{aligned}\quad (10)$$

where a prime denotes the derivative of a function with respect to its lone argument, a subscript ‘-’ indicates a quantity evaluated on the core side of the interface, and a subscript ‘+’ indicates a quantity evaluated on the envelope side of the interface.

The equilibrium in both regions is governed by the Lane-Emden equation,

$$\frac{1}{\xi^2} (\xi^2 \psi')' = \exp(-\psi). \quad (11)$$

The unique solution of equation (11), subject to the standard (i.e. regular) boundary conditions,

$$\psi = 0, \quad \psi' = 0 \quad \text{at} \quad \xi = 0,$$

is the isothermal function tabulated by Chandrasekhar & Wares (1949). Thus, for a given dimensionless core radius, $\xi_i = r_i/r_{\text{ch}}$, ψ_- , and ψ'_- are known (a subscript i denotes quantities that are continuous across the interface). Equations (10) are then three equations in three unknowns: ψ_+ , ψ'_+ , and ρ_e/ρ_c . Solving these, one obtains the following relations:

$$\psi_+ = \psi_- + 2 \ln \tau_i, \quad \psi'_+ = \psi'_-/\tau_i, \quad \rho_e/\rho_c = \tau_i. \quad (12)$$

Equations (12) give starting values for the integration of equation (11) out to some radius $r_s \equiv r_{\text{ch}} \xi_s$, where an outer boundary condition is imposed. We imagine that the composite cloud is ultimately surrounded by a tenuous (compared to the envelope) intercloud medium, whose entire dynamical effect is to exert a finite, constant pressure everywhere on the outer boundary. This situation is effectively the same as is assumed for the well-known bounded isothermal sphere (Ebert 1955; Bonnor 1956) except that we suppose P_s to be comprised of both thermal and nonthermal components. Using equations (5), (6), (9) and (12), we find that this pressure is related to the central pressure, $P_c = c_{\text{core}}^2 \rho_c$, via

$$\frac{P_c}{P_s} = \tau_i^{-2} \exp(\psi_s). \quad (13)$$

Note that the corresponding density contrast is simply $\tau_i(P_c/P_s)$. Alternatively, one may specify a given configuration by its ratio of core-to-total radius and/or mass. The definitions of M and r along with equations (12) yield

$$\begin{aligned}\frac{r_i}{r_s} &= \frac{\xi_i}{\xi_s}, \\ \frac{M_i}{M_s} &= \tau_i^{-1} \frac{(\xi_i^2 \psi')_-}{(\xi_s^2 \psi')_s}.\end{aligned}\quad (14)$$

Note that when expressing products of quantities, any one of which is not continuous across the interface, we retain the ‘-’ subscripts for the entire product.

2.5. Isothermal Cores with Polytrropic Envelopes

We next consider composite polytropes with isothermal cores and polytrropic envelopes as an approximate model for molecular clouds. (In principle, the core of a composite polytrope can have an arbitrary polytrropic index, but we restrict consideration here to the special case in which it is isothermal.) As remarked above, composite polytropes have long been used in studies of stellar structure. The general matching conditions for two-component spheres of differing polytrropic indices n were presented by Chandrasekhar (1939).

The Lane-Emden equation governing the envelope is

$$\frac{1}{\xi^2} (\xi^2 \theta')' = \Delta \theta^n, \quad \Delta \equiv -\frac{|n+1|}{n+1} = \pm 1, \quad (15)$$

where the suitably non-dimensionalized variables for the envelope are

$$\begin{aligned}\rho &= \rho_e \theta^n, \quad P = K_{\text{env}} \rho^{1+1/n} = K_{\text{env}} \rho_e^{1+1/n} \theta^{n+1}, \\ r &= \left[\frac{|n+1|}{4\pi G} K_{\text{env}} \rho_e^{1/n-1} \right]^{1/2} \xi, \\ M(r) &= 4\pi \Delta \rho_e r_{\text{ch}}^3 \xi^2 \theta',\end{aligned}$$

where we have used the continuity of ξ to express the mass in terms of characteristic radius for the isothermal core, r_{ch} . Recall that n and γ_p are related via $\gamma_p = 1 + 1/n$. The matching conditions at the core-envelope interface are

$$\begin{aligned}c_{\text{core}}^2 \rho_c \exp(-\psi_-) &= K_{\text{env}} \rho_e^{1+1/n} \theta_+^{n+1}, \\ c_{\text{core}} \rho_c^{-1/2} &= (|n+1| K_{\text{env}} \rho_e^{1/n-1})^{1/2}, \\ \rho_c \psi'_- &= \Delta \rho_e \theta'_+.\end{aligned}\quad (16)$$

Generalizing the definition of τ_i (eq. 5) to the case of a polytrropic envelope, we have

$$\tau_i \equiv \frac{c_+^2}{c_{\text{core}}^2} = \frac{\rho_-}{\rho_+} = \frac{\rho_c \exp(-\psi_-)}{\rho_e \theta_+^n}. \quad (17)$$

The first two of equations (16) can be combined to give

$$\left(\frac{\rho_e}{\rho_c} \right)^2 \exp(\psi_-) \theta_+^{n+1} = |n+1|. \quad (18)$$

Equations (16)–(18) then yield the jump conditions:

$$\begin{aligned}\theta_+ &= [\tau_i^2 |n+1| \exp(\psi_-)]^{1/(1-n)}, \\ \theta'_+ &= \Delta \tau_i \psi'_- \exp(\psi_-) \theta_+^n, \\ \rho_e/\rho_c &= \tau_i^{-1} \exp(-\psi_-) \theta_+^{-n}.\end{aligned}\quad (19)$$

These are the equivalents of equations (12) in the case of a polytrropic envelope.

The ratio of core-to-total radius is again given by equation (14), while the mass ratio is

$$\frac{M_i}{M_s} = \Delta \tau_i \exp(\psi_-) \theta_+^n \frac{(\xi^2 \psi')_-}{(\xi^2 \theta')_s}.$$

Finally, the center-to-surface pressure and density contrasts are given by

$$\begin{aligned} \frac{P_c}{P_s} &= |n+1| [\tau_i \exp(\psi_-) \theta_+^n]^2 \theta_s^{-n-1} \\ \frac{\rho_c}{\rho_s} &= \tau_i \exp(\psi_-) (\theta_+ / \theta_s)^n. \end{aligned} \quad (20)$$

As discussed in §§2.2-2.3 above, the adiabatic indexes for both core and envelope are expected to be less than 4/3. As a result, the composite polytrope must be bounded by a medium of finite and constant pressure at its surface (MH). Also note that the envelope temperature $T \propto P/\rho \propto \rho^{1/n}$ is an increasing function of ξ in NIPs (Shu et al 1972; Viala & Horedt 1974). As mentioned in §2.3, we interpret the departure from isothermality in the envelope as arising entirely from the presence of mean magnetic fields and Alfvénic turbulence, approximated as isotropic pressure components. The latter appear as nonthermal contributions to the total sound speed, given by (McKee & Zweibel 1995)

$$c^2(r) \equiv \frac{P(r)}{\rho(r)} = \sigma_{\text{th}}^2 + \frac{3}{2} \sigma_w^2(r) + \frac{1}{2} v_A^2(r), \quad (21)$$

where σ_{th} is the (constant) thermal speed, $\sigma_w(r)$ is the velocity dispersion associated with Alfvén waves, and $v_A(r) \equiv B(r)/\sqrt{4\pi\rho(r)}$ is the Alfvén speed. In our model, σ_w is the same as the nonthermal velocity dispersion σ_{nt} . Note that the total velocity dispersion is related to $c(r)$ by

$$\sigma(r) = [\sigma_{\text{th}}^2 + \sigma_w^2(r)]^{1/2} = \left[\frac{2}{3} c^2(r) + \frac{1}{3} \sigma_{\text{th}}^2 - \frac{1}{3} v_A^2(r) \right]^{1/2}. \quad (22)$$

2.6. Stability of Composite Configurations

While polytropic models of molecular clouds clearly represent a simplification of the real situation, they have a distinct advantage over more detailed models, in that the analysis of their stability is straightforward. We note, however, that previous studies disagree as to whether such a cloud responds isothermally or adiabatically to radial perturbations applied at its surface. We review this situation in the Appendix, and justify our choice of the adiabatic stability criterion adopted here.

The equation of radial motion for small, adiabatic perturbations about equilibrium is, quite generally (Eddington 1926; Ledoux & Walraven 1958)

$$\begin{aligned} \frac{d^2 h}{dr^2} + \left[\frac{4}{r} + \frac{1}{\gamma} \frac{d\gamma}{dr} - \frac{GM(r)\rho}{r^2 P} \right] \frac{dh}{dr} \\ + \left[\frac{\omega^2 \rho}{\gamma P} + \frac{3}{\gamma r} \frac{d\gamma}{dr} - \left(3 - \frac{4}{\gamma} \right) \frac{GM(r)\rho}{r^3 P} \right] h = 0, \end{aligned} \quad (23)$$

where $h \equiv \delta r/r$ is the relative displacement of a fluid element at a radius r and ω is the frequency of the oscillations. We assume that the adiabatic index, γ , can take on any (positive and constant) value in either the core or the envelope. Thus, in general, γ has a discontinuity at the interface. For the reasons outlined § 1.2, we confine our interest to critically stable clouds, setting $\omega = 0$ in what follows.

Under these assumptions, equation (23) becomes, in the isothermal core,

$$\frac{d^2 h_{\text{core}}}{d\xi^2} + \left(\frac{4}{\xi} - \psi' \right) \frac{dh_{\text{core}}}{d\xi} - (3 - 4/\gamma_{\text{core}}) \frac{\psi'}{\xi} h_{\text{core}} = 0 \quad (\text{isothermal}). \quad (24)$$

When $\gamma_{\text{core}} = 1$, Yabushita (1974) showed that there exists an exact solution of equation (24); namely,

$$h_{\text{core}}(\xi) = \epsilon \left[\frac{\psi'}{\xi} \exp(\psi) - 1 \right],$$

where ϵ is a small, dimensionless constant.

The solution of equation (24) must be matched onto the corresponding solution in the envelope, $h = h_{\text{env}}$. For an isothermal envelope, the governing equation is identical in form to equation (24); for a polytropic envelope, one has

$$\begin{aligned} \frac{d^2 h_{\text{env}}}{d\xi^2} + \left[\frac{4}{\xi} + (n+1) \frac{\theta'}{\theta} \right] \frac{dh_{\text{env}}}{d\xi} \\ + (3 - 4/\gamma_{\text{env}})(n+1) \frac{\theta'}{\theta \xi} h_{\text{env}} = 0 \quad (\text{polytropic}). \end{aligned} \quad (25)$$

By definition, h must be continuous at the interface; i.e. $h_{\text{env}}(\xi_i) = h_{\text{core}}(\xi_i)$. Its derivative must satisfy the condition (Ledoux & Walraven 1958)

$$\left(\frac{dh_{\text{env}}}{d\xi} \right)_+ = \frac{\gamma_{\text{core}}}{\gamma_{\text{env}}} \left(\frac{dh_{\text{core}}}{d\xi} \right)_- + \frac{3h_{\text{core}}}{\xi_i} \left(\frac{\gamma_{\text{core}}}{\gamma_{\text{env}}} - 1 \right),$$

which takes into account the possibility of a discontinuity in γ across the interface.

The condition for the critical point is that the Lagrangian variation in the pressure at the boundary vanish, $(\delta P/\delta r)_{M_s} = 0$ (Ledoux & Walraven 1958; MH). This places the following restriction on h_{env} :

$$\left(\frac{dh_{\text{env}}}{d\xi} + 3 \frac{h_{\text{env}}}{\xi} \right)_{\xi=\xi_s} = 0. \quad (26)$$

This condition holds for both isothermal and polytropic envelopes, and differs from those expressed by equations (13) and (20), in that it holds *only* for critically stable states. Finally, note that although we shall take $n < -1$ ($0 < \gamma_p < 1$) in what follows, the results of this section hold for all $n \neq -1$.

2.7. Solution Procedure

In practice, the solution procedure for critical states is as follows:

- (1) Choose a model by specifying five parameters: n (or γ_p), γ_{core} , γ_{env} , ξ_i , and τ_i .
- (2) Solve the Lane-Emden equation for an isothermal sphere on the interval $[0, \xi_i]$; i.e., find $\psi(\xi)$ and ψ' .
- (3) Using ψ_- , ψ'_- , $h_{\text{core}}(\xi_i)$, and $(dh_{\text{core}}/d\xi)_-$ as starting values, calculate θ_+ , θ'_+ , $h_{\text{env}}(\xi_i)$, and $(dh_{\text{env}}/d\xi)_+$. These are the starting values for the integration of the two ODES (11) and (24) (isothermal envelope) or (15) and (25) (polytropic envelope).
- (4) Integrate the system outward in ξ until the outer boundary condition (26) is satisfied.

The resulting unique solution yields, as dimensionless output parameters: (i) the center-to-surface pressure and density contrasts; (ii) the core-to-total radius ratio; and (iii) the core-to-total mass ratio.

3. SINGLE-COMPONENT POLYTROPES: A REVIEW

Consider the variation of the mass M of a single-component NIP ($-\infty < n < -1$; $0 < \gamma_p < 1$) if the surface pressure and entropy are held fixed while the central density is increased. For fixed surface conditions, the behavior of M follows that of the dimensionless mass μ defined by MH,

$$\mu \equiv \frac{M}{c_s^4/(G^3 P_s)^{1/2}} = \frac{M}{c_s^3/(G^3 \rho_s)^{1/2}}. \quad (27)$$

The sequence of μ versus ρ_c/ρ_s ranges from zero at $\rho_c/\rho_s = 1$ up to some maximum μ_{\max} , beyond which it oscillates about the value corresponding to a singular polytropic sphere as $\rho_c/\rho_s \rightarrow \infty$ (Chandrasekhar 1939; MH), i.e.

$$\mu_\infty = \left(\frac{2}{\pi}\right)^{1/2} \frac{(4-3\gamma_p)^{1/2} \gamma_p^{3/2}}{(2-\gamma_p)^2} = \left(\frac{2}{\pi}\right)^{1/2} \frac{|n-3|^{1/2} |n+1|^{3/2}}{(n-1)^2}.$$

The sequence is qualitatively similar for all values of $0 < \gamma_p < 6/5$: the maximum possible mass of a polytrope in this range is determined by the conditions at its surface. (The same conclusion holds if c_s is replaced by the rms value $\langle c^2 \rangle^{1/2}$.)

The largest *stable* density drop along this sequence occurs at the critical mass μ_{cr} , which is less than or equal to μ_{\max} . In the isentropic case, $\gamma = \gamma_p$, one has $\mu_{\text{cr}} = \mu_{\max}$ (Shu et al 1972). In this case, all higher density, lower mass models are gravitationally unstable. When $\gamma > \gamma_p$, $\mu_{\text{cr}} < \mu_{\max}$, even though the corresponding $(\rho_c/\rho_s)_{\text{cr}}$ is greater than in the isentropic case. This behavior is illustrated in Figure 1, which displays the partial equilibrium sequences of both an $n = -3$ ($\gamma_p = 2/3$) polytrope and the isothermal sphere. Recall that when $\gamma < \gamma_p$, both polytropic and isothermal spheres are convectively unstable, according to the Schwarzschild criterion (Cowling 1941).

Sometimes we know the conditions at the *center* of the polytrope, and can ask how much mass can be supported. In this case, the equilibrium mass can increase without limit as the surface pressure and density are lowered (Viala & Horedt 1974); however, such equilibria are stable only if they are sufficiently non-isentropic. Noting that $c_s^2 = P_s/\rho_s \propto \rho_s^{1/n}$, we have $M \propto \mu \rho_s^{(3-n)/2n}$; as $\rho_s/\rho_c \rightarrow 0$ for fixed ρ_c , $\mu \rightarrow \mu_\infty$ and $M \rightarrow \infty$ for $n > 3$ and $n < -1$ ($0 \leq \gamma_p < 4/3$).

4. THE COMPOSITE ISOTHERMAL SPHERE

4.1. Pressure and Density Structure

In Figures 2a and b, we plot, for various values of τ_i , the critical density contrast of the composite isothermal sphere (CIS), $(\rho_c/\rho_s)_{\text{CI,cr}}$, as a function of r_i/r_s and M_i/M_s , respectively. We first present results for the isentropic case only, i.e. $\gamma_{\text{core}} = \gamma_{\text{env}} = \gamma_p = 1$. Note that the corresponding pressure contrasts are simply a factor of τ_i lower than $(\rho_c/\rho_s)_{\text{CI,cr}}$. The left-hand border of Fig. 2 corresponds to the case of an almost pure envelope with a core at the origin, whereas the right-hand border corresponds to the case of an almost pure core with an envelope at the surface. In each case, the limiting values of the curves at the borders are $(\rho_c/\rho_s)_{\text{CI,cr}} \rightarrow \tau_i (\rho_c/\rho_s)_{\text{BE}}$, indicating that $(P_c/P_s)_{\text{CI,cr}} \rightarrow (P_c/P_s)_{\text{BE}}$, as expected. Note that for values

of $\tau_i \gtrsim 5$, configurations with the *same* r_i/r_s can have *different* $(\rho_c/\rho_s)_{\text{CI,cr}}$. These equilibria are still unique, however, as evidenced from the absence of this feature in Fig. 2b, which employs the Lagrangian variable M_i/M_s .

For each value of τ_i , there is a maximum in $(\rho_c/\rho_s)_{\text{CI,cr}}$, which increases with increasing τ_i . As $\tau_i \rightarrow \infty$, the density contrast across the interface becomes infinite, and thus an infinite center-to-edge density contrast can be supported. The maximum *pressure* contrast, however, is finite, and can be estimated as follows. Since the core becomes less important with increasing τ_i (it is already only 5% of the total radius and 1% of the total mass at $\tau_i = 5$), one can view this region in the large- τ_i limit as a tiny, cold and dense ‘‘pea’’ in the midst of an essentially infinite, hot and tenuous background. These are precisely the conditions pertaining to the bounded isothermal sphere. Thus, on the scale at which pressure gradients in the core are significant, $\xi \lesssim \xi_i$, the maximum pressure contrast across the core alone will be $(P_c/P_i)_{\text{cr}} \approx (P_c/P_s)_{\text{BE}}$. On the other hand, on the scale at which pressure gradients in the envelope are significant, $\xi \gg \xi_i$, the region within the core is essentially structureless; its only significance for the equilibrium is to set the interface values of various quantities. Thus, the expected maximum pressure contrast in the envelope alone will again approach the Bonnor-Ebert value. Together, these results imply a *total* pressure contrast in the large- τ_i limit of

$$\left(\frac{P_c}{P_s}\right)_{\text{CI,cr}} = \left(\frac{P_c}{P_i}\right)_{\text{cr}} \left(\frac{P_i}{P_s}\right)_{\text{cr}} \approx \left(\frac{P_c}{P_s}\right)_{\text{BE}}^2 \simeq 197.$$

The critical stability curves of pressure contrast versus r_i/r_s do indeed approach this asymptotic limit for $\tau_i \gg 1$ (Fig. 2c). Correspondingly, the total pressure contrast for a composite polytrope consisting of N components, each separated from the other by a large value of τ_i , approaches $(14.04)^N$.

4.2. Radius and Mass

The dimensionless outer radius of the critical CIS can be much larger than that of the Bonnor-Ebert sphere; e.g. when $\tau_i = 2$ and $r_i/r_s = 0.1$, it extends to $\xi_{\text{CI,cr}} = 15.7$, versus $\xi_{\text{BE}} = 6.45$. Note that $\xi_{\text{CI,cr}}$ is a function of the core-to-total radius ratio r_i/r_s . As this ratio approaches zero (i.e., a pure envelope), one finds that $\xi_{\text{CI,cr}} \rightarrow \tau_i \xi_{\text{BE}}$, or $\xi_{\text{CI,cr}} = 12.9$ in the case considered here. Hence, the outer radius attains a maximum at some intermediate r_i/r_s .

Because the temperatures of the densest observed regions of molecular clouds consistently fall in the range 10-20 K, it is convenient to normalize the mass with respect to this value rather than the surface value. On the other hand, the pressure at the surface of a cloud is dictated by the ambient conditions, and is often better determined than the pressure in the cloud interior. We therefore introduce a hybrid dimensionless mass based on the temperature in the core and the pressure at the surface of the envelope:

$$m(r) \equiv \frac{M(r)}{c_{\text{core}}^4/(G^3 P_s)^{1/2}}. \quad (28)$$

For fixed c_{core} and P_s , $m(r)$ is directly proportional the dimensional mass $M(r)$. By contrast, the dimensionless mass μ introduced above is normalized to the characteristic Jeans mass at r ; the two are related by

$$\frac{\mu(r)}{m(r)} = \frac{c_{\text{core}}^4}{c^4(r)} \left[\frac{P(r)}{P_s}\right]^{1/2} = \frac{1}{\tau^2} \left[\frac{P(r)}{P_s}\right]^{1/2}, \quad (29)$$

where

$$\tau \equiv \frac{c^2}{c_{\text{core}}^2}.$$

For a CIS, $\tau = 1$ in the core and $\tau = \tau_i$ in the envelope.

The total dimensionless mass of a composite isothermal sphere is then

$$m_{CI} = m_{\text{core}} + m_{\text{env,I}}, \quad (30)$$

where

$$m_{\text{core}} \equiv \frac{P_s^{1/2} G^{3/2}}{c_{\text{core}}^4} M_{\text{core}} = \left(4\pi \frac{P_c}{P_s}\right)^{-1/2} (\xi^2 \psi')_- \quad (31)$$

$$m_{\text{env,I}} \equiv \frac{P_s^{1/2} G^{3/2}}{c_{\text{core}}^4} M_{\text{env,I}} = \left(4\pi \frac{P_c}{P_s}\right)^{-1/2} \tau_i [(\xi^2 \psi')_s - (\xi^2 \psi')_+].$$

In the limit that the CIS is a pure core ($r_i/r_s \rightarrow 1$, $\xi_- \rightarrow \xi_s$), $m_{CI} = m_{\text{core}}$ must approach m_{BI} , the dimensionless mass of the bounded isothermal sphere,

$$m_{BI} = \frac{P_s^{1/2} G^{3/2}}{c^4} M = \left(4\pi \frac{P_c}{P_s}\right)^{-1/2} (\xi^2 \psi')_{BI,s}. \quad (32)$$

The last step, which follows from equations (7) and (8), shows that m_{BI} indeed agrees with m_{core} from equation (31) in this limit. In the opposite limit in which the CIS is a pure envelope ($r_i/r_s \rightarrow 0$, $\xi_+ \rightarrow 0$), equation (29) implies $m_{CI} \rightarrow (c/c_{\text{core}})^4 m_{BI} = \tau_i^2 m_{BI}$. The maximum mass of the CIS occurs for the pure envelope (see Figure 3), and since $m_{BI} \leq m_{BE}$, we find that the upper limit on the mass of a CIS is

$$m_{CI} \leq \tau_i^2 m_{BE}. \quad (33)$$

The above expressions are also valid for the critically stable CIS. The critically stable pure core or envelope is the Bonnor-Ebert sphere with $\mu_{BE} = m_{BE} = 1.1822$. Note that because the critical values of P_i/P_s , m_{core} , and $m_{\text{env,I}}$ depend on the fractional core radius r_i/r_s , $m_{CI,\text{cr}}$ is a function of r_i/r_s . We plot $m_{CI,\text{cr}}/m_{BE}$, in the isentropic case, for various values of τ_i in Figures 3a and b. The individual core and envelope components are also shown. Note that in general, as τ_i increases, the core becomes a lesser contributor to the overall mass of the cloud. As $\tau_i \rightarrow \infty$, we recover the pure envelope case. Finally, note that the above mass expressions are quite general; they apply to both isentropic ($\gamma = \gamma_p$) and non-isentropic ($\gamma \neq \gamma_p$) spheres.

4.3. The Non-isentropic CIS

Consider now the much larger class of non-isentropic, critical CISs; i.e. those with $\gamma \neq 1$. We are most interested in the range $1 < \gamma < 4/3$, as discussed in §2.3. Single-component isothermal spheres with γ in this range were examined by Yabushita (1968), who showed that the dimensionless critical radius and pressure contrast of such spheres approached infinity as $\gamma \rightarrow 32/25$. The critical radius and pressure contrast remain infinite for $32/25 < \gamma < 4/3$ (MH).

These features of single-component spheres can largely be carried over to the CIS. That is, CISs with $\gamma_{\text{core}} > 1$ and/or $\gamma_{\text{env}} > 1$ have pressure contrasts in excess of those found in the isentropic case, but smaller masses. The maximum pressure contrasts (i.e., as a function of r_i/r_s) for CISs with $\tau_i = 2$ and $\tau_i = 3$ are plotted as contours in the $(\gamma_{\text{core}}, \gamma_{\text{env}})$ plane in Figures 4a and b. Note that as γ_{core} and γ_{env} approach the value 32/25, the various physical quantities diverge, and it proves difficult to

integrate the equations all the way up to the singular point. This is a feature of Fig. 4 and several of our subsequent plots; however, we need not be concerned that any essential qualitative behavior is being missed.

To outline the important qualitative changes in the non-isentropic CIS, let us restrict consideration to $\tau_i = 1$ and $1 < \gamma \lesssim 1.25$. Then the critical mass extrema always obtain in the limit of a pure core or envelope, depending on the relation between γ_{core} and γ_{env} . If $\gamma_{\text{core}} > \gamma_{\text{env}}$, then the minimum (maximum) mass is given by a pure core (envelope); and conversely if $\gamma_{\text{core}} < \gamma_{\text{env}}$. Further, these extrema are given by the usual bounded isothermal sphere sequence beyond the mass peak (Fig. 1). When $\tau_i > 1$ and/or γ_{core} or $\gamma_{\text{env}} \gtrsim 1.25$, the mass extrema no longer necessarily occur for a pure core or envelope: the values of r_i/r_s corresponding to the mass peak depend on the exact values of τ_i , γ_{core} , and γ_{env} . As previously discussed, $\gamma_{\text{env}} > 1 \Rightarrow m_{\text{env,I}} < m_{BE}$, even in the pure envelope limit. On the other hand, for $\tau_i > 1$, this effect competes with a relatively larger mass contribution from the envelope, due to its increased temperature (§4.2). This combination sometimes leads to a maximum in $m_{CI,\text{cr}} (\leq m_{BE})$ at intermediate r_i/r_s , an effect manifested by the slight asymmetry in the $(P_c/P_s)_{CI,\text{cr}}^{\text{max}}$ contours between corresponding pairs of $(\gamma_{\text{core}}, \gamma_{\text{env}})$ in Fig. 4a.

4.4. Summary—CIS

Whereas the bounded isothermal sphere (usually assumed to be isentropic, so that $\gamma = 1$) has a maximum density and pressure contrast between the center and the surface of a factor 14.04, composite isothermal spheres can have much larger drops: for two components with a temperature jump τ_i , the pressure drop can be up to a factor $(14.04)^2 = 197$ (in the limit of large τ_i), and the density drop a factor τ_i larger. Non-isentropic isothermal spheres, whether composite or not, can have very large density and pressure drops provided γ is close to 4/3. We attribute the increased stability of composite polytropes and non-isentropic polytropes to the fact that they both have an entropy that increases outwards. The entropy is proportional to $\ln(P/\rho^\gamma)$, which increases outward as $(\gamma - \gamma_p) \ln(\rho_c/\rho)$ for a non-isentropic polytrope and as $\gamma \ln \tau_i$ across a jump in a composite polytrope.

The core mass of a CIS can never exceed its Bonnor-Ebert mass ($m_{\text{core}} \leq m_{BE} = 1.18$), and the mass of the entire CIS can never exceed the Bonnor-Ebert mass of the envelope ($\mu_{CI} \leq 1.18$). As shown in Fig. 3 and in equation (33), however, the dimensionless mass of the CIS can exceed m_{BE} whenever $\tau_i > 1$, since $m_{CI,\text{cr}} \rightarrow \tau_i^2 m_{BE}$ in the limit of a pure envelope. The dimensionless mass of a non-isentropic CIS is less than that of an isentropic one (with the same τ_i).

In order to compare the mass of a CIS with that of an actual dense core or globule, we need to re-express equation (30) in dimensional form. Scaling to the representative values $T_{\text{core}} = 10$ K and $P_s/k = 2 \times 10^4 \text{ cm}^{-3} \text{ K}$ (Boulares & Cox 1990; we have subtracted the cosmic ray pressure, since cosmic rays penetrate the molecular gas as well), one finds

$$M_{CI} = \frac{c_{\text{core}}^4}{P_s^{1/2} G^{3/2}} m_{CI} = 2.2 M_{\odot} \left(\frac{T_{\text{core}}}{10 \text{ K}}\right)^2 \times \left(\frac{2 \times 10^4 \text{ cm}^{-3} \text{ K}}{P_s/k}\right)^{1/2} m_{CI}, \quad (34)$$

where a mean molecular weight of $2.33 m_H$ has been assumed. The quantity m_{CI} , scaled by m_{BE} , can be read off from Fig.

3. Assuming these representative values, the mass of the isentropic, critical CIS falls within the range $2.6 M_\odot \leq M_{C,cr} \leq 2.6 \tau_i^2 M_\odot$ (see eq. 33). The total molecular masses of dense cores and globules derived from ammonia and $C^{18}O$ measurements range between a few M_\odot and a few tens of M_\odot (§1.1), so critical CISs with $\tau_i \lesssim 5$ are in good agreement on this count.

Since observations show that PPCs and Bok globules both have substantial nonthermal motions in their envelopes, CISs are primarily of academic interest. We turn now to the more realistic case in which the envelope has a substantial nonthermal pressure.

5. THE COMPOSITE POLYTROPIC SPHERE

In models having a polytropic envelope, we assume that the thermal velocity in the envelope is the same as that in the core, $\sigma_{th,env} = \sigma_{th,core}$. The polytropic temperature, $T(r) \propto c^2(r)$, may be interpreted as the sum of the kinetic temperature, T_{kin} (fixed at the core value, T_{core}), and an “effective” temperature, $T_{eff}(r) \propto (3\sigma_w^2 + v_A^2)/2$ (see eq. 21). At the inner edge of the envelope, $T_{eff,+} = (\tau_i - 1) T_{core}$, so that when $\tau_i > 1$, the jump in T across the interface is assumed to be *entirely* due to a nonzero value of $T_{eff}(r_i)$.⁶ We focus on the case of NIPs for the envelope ($n < -1$, $0 < \gamma_p < 1$).

5.1. Pressure and Density Structure

Beginning again with the isentropic case, in Figure 5a we plot, for various negative values of n and for $\tau_i = 1$, the critical density and pressure contrasts of the composite polytropic sphere (CPS). In Figs. 5b and c, results are given for $\tau_i = 2$ and $\tau_i = 3$, respectively. For $\tau_i = 1$, these curves approach the correct values for pure polytropes at $r_i/r_s = 0$ (Shu et al 1972)⁷ and the Bonnor-Ebert value at $r_i/r_s = 1$. For $\tau_i > 1$, the density curves approach τ_i times these same limiting values. Observe that CPSs attain peak critical densities that are typically a few times larger than their pure polytropic counterparts for $\tau_i = 1$, and up to an order of magnitude (or more) larger for $\tau_i \gtrsim 2$. Also note that for $\tau_i > 1$ and $|n|$ sufficiently larger than 1 (i.e., $\gamma_p \rightarrow 1$), $(P_c/P_s)_{cr}$ can exceed $(P_c/P_s)_{BE}$ for a finite range of r_i/r_s , just as in the case of the CIS (see Fig. 2c).

Fig. 5 also shows that the limit $n \rightarrow -1$ ($\gamma_p \rightarrow 0$) is quite anomalous, in that the density contrast (but not the pressure contrast) greatly exceeds that of other CPSs over a large range of r_i/r_s . This can be understood as follows: For small r_i/r_s , the CPS is mostly constant-pressure envelope, and is thus highly unstable. But as r_i/r_s increases, stability is recovered due to the presence of the isothermal core. More importantly, the high compressibility of the $n \simeq -1$ envelope has two distinct and complementary effects: first, the core is relatively insensitive to perturbations occurring at the cloud surface; and second, a relatively small pressure drop across the envelope corresponds to a large density drop. As in previous cases, these effects are only enhanced when $\tau_i > 1$.

5.2. Radius and Mass

As in the case of the CIS, the dimensionless outer radius of the critical CPS has a maximum at an intermediate value of r_i/r_s . This maximum is always greater than the Bonnor-Ebert critical radius, and therefore also greater than $\xi_{P,cr}$, the critical radius of the pure polytrope (Shu et al 1972). As $r_i/r_s \rightarrow 0$ (i.e.,

a pure envelope), one finds that $\xi_{CP,cr} \rightarrow \tau_i^{(n+1)/2n} |n+1|^{1/2} \xi_{P,cr}$; e.g., $\xi_{CP,cr} = 6.77$ when $n = -3$ and $\tau_i = 2$.

The mass of the CPS, in dimensionless form, is

$$m_{CP} = m_{core} + m_{env,P},$$

where m_{core} is given by equation (31),

$$m_{env,P} \equiv \frac{P_s^{1/2} G^{3/2}}{c_{core}^4} M_{env,P} = \left(4\pi \frac{P_c}{P_s} \right)^{-1/2} \Delta\tau_s \frac{|n+1|}{\theta_s} \times [(\xi^2\theta')_s - (\xi^2\theta')_+],$$

and $\tau_s \equiv \tau(r_s) = c_s^2/c_{core}^2$. In the limit that the CPS is a pure core, one again obtains $m_{CP} \rightarrow m_{BI}$, while in the pure envelope limit,

$$m_{CP} = m_{env,P} \rightarrow \tau_s^2 m_P, \quad (35)$$

where $m_P \equiv (P_s^{1/2} G^{3/2}/c_s^4) M$ is the polytropic analog of m_{BI} for a polytropic sphere. Note, once again, the factor of τ_s^2 that enters since m_{CP} is normalized to c_{core} .

The critical mass of the CPS is plotted in the isentropic case for various envelope indices and $\tau_i = 1$ in Figure 6. Note the asymptotic approach to the Bonnor-Ebert mass of the core at $r_i/r_s = 1$, and the different limiting values (according to n) at $r_i/r_s = 0$. The latter values, which are for pure envelopes, differ from those of Shu et al (1972) due to the difference in non-dimensionalization. Their values are normalized to the surface temperature so that the critical mass is always *less* than the Bonnor-Ebert mass (i.e. $\mu_{P,cr} < \mu_{BE} = m_{BE}$ for NIPs), whereas our values are normalized to the central temperature, and thus (for pure envelopes) $m_{P,cr}$ can exceed m_{BE} . The critical mass of a pure polytrope has a maximum of $m_{P,cr} \simeq 1.4 m_{BE}$ at $n = -2.90$ ($\gamma_p = 0.655$); this is in fact the maximum for *all* isentropic CPSs. CPSs with $-2.12 \leq n < -1$ have a maximum in $m_{CP,cr}$ at intermediate r_i/r_s . In the limit of a constant pressure polytrope, $n \rightarrow -1$ ($\gamma_p \rightarrow 0$), the critical mass shrinks to zero as the pressure gradient vanishes, while the mass for $|n| \gtrsim 100$ is essentially constant at the Bonnor-Ebert value for all r_i/r_s .

In Figures 7a and b, we focus on the fiducial envelope index $n = -3$ ($\gamma_p = 2/3$) in order to examine the behavior of the critical mass as a function of τ_i . Note the similarity of these curves to those of the CIS, shown in Fig. 3. The “loops” appearing in Fig. 7a for $\tau_i \gtrsim 3$, which mark the end of the envelope’s dominant mass contribution, indicate that configurations with the same fractional core radius can have different critical masses. As in the case of the CIS (§4), this multi-valuedness disappears in a plot of $m_{CP,cr}$ versus the fractional core mass, M_i/M_s (Fig. 7b).

5.3. Velocity Dispersion

The observable component of the sound speed, $c(r)$, is the velocity dispersion, $\sigma(r)$, given by equation (22). The structure of the equilibrium CPS gives $P(r)$ and $\rho(r)$, so $c(r)$ is easily calculated from equation (21). In order to gain a qualitative feel for $\sigma(r)$ and for the nonthermal velocity dispersion, $\sigma_{nt}(r) = \sigma_w(r)$, we set $v_A = 0$ and plot these quantities for an isentropic CPS with $n = -3$, $\tau_i = 1$, and various values of r_i/r_s in Figure 8a. Also plotted are the same quantities for a pure $n = -3$ polytrope, with the central dispersion normalized to c_{core} . Outside

⁶In some cases, e.g., Bok globules exposed to the interstellar radiation field, the kinetic temperature may increase outward. Then, an assumed $T_{kin}(r)$ gives $\sigma_{th}(r)$ and $T_{eff}(r) = T(r) - T_{kin}(r)$.

⁷Note, however, the following error in Shu et al’s Table 4. While $(P_c/P_s)_{cr} \rightarrow 1$ as $n \rightarrow -1$, this is not true of $(\rho_c/\rho_s)_{cr}$; rather, $(\rho_c/\rho_s)_{cr} \rightarrow 5.13$ in this limit (MH).

of the thermal core, both dispersions increase monotonically with radius. Note how the slope of the nonthermal dispersion in the envelope increases with increasing core fraction. Fig. 8b shows how, in certain cases (here for $n = -1.5$, corresponding to $\gamma_p = 1/3$), both σ and its slope can exceed the pure polytropic values for a finite range of r_i/r_s (here $0.2 \lesssim r_i/r_s \lesssim 0.55$). This behavior will become increasingly important once we set out to model the observed increase of linewidth with size.

In order to compare these model velocity dispersions with the observed molecular linewidths, one must first calculate the *projected* linewidth through the region of the cloud having $n > n_{\text{cr}}$, where n_{cr} is the critical density for the excitation of a given molecular line (e.g. Genzel 1992). We will discuss this procedure more fully, and present detailed modeling, in a subsequent paper.

5.4. The Non-isentropic CPS

The CPS offers an improvement over the CIS, in that it is qualitatively consistent with the observed increase of velocity linewidth with size in molecular clouds. But, as is evident from the critical masses plotted in Fig. 6, the isentropic CPS shares a common problem with the CIS in that it cannot *quantitatively* reproduce the observed mass range of PPCs; in order to obtain masses and density contrasts that are as large as those inferred, one requires $\tau_i \gtrsim 3$, a jump in c^2 for which there is neither theoretical nor observational justification. As we have argued, insofar as molecular clouds can be described as polytropes, they are more likely to be non-isentropic in character. It is therefore of some benefit to examine the quantitative properties of such polytropes.

The theory of single-component, non-isentropic polytropes was reviewed and extended by MH. They showed that, for a given γ_p (or n), the value of $(\rho_c/\rho_s)_{\text{cr}}$ increases as γ increases above γ_p , and reaches infinity at a well-defined value $\gamma = \gamma_\infty$, given by

$$\gamma_\infty = \frac{32\gamma_p(2-\gamma_p)}{(6-\gamma_p)^2} = \frac{32(n^2-1)}{(5n-1)^2}, \quad (36)$$

corresponding to the family of singular polytropic configurations. Observe that in the isothermal case ($\gamma_p = 1$, $n = \pm\infty$), $\gamma_\infty = 32/25$, as found by Yabushita (1968).

Again focussing on the fiducial value $n = -3$, in Figures 9a and b we plot contours of maximum density contrast, $(\rho_c/\rho_s)_{\text{cr}}^{\text{max}}$, for $\tau_i = 1$ and $\tau_i = 2$. Recall that these maxima occur for different values of r_i/r_s , depending on the exact values of τ_i , γ_{core} , and γ_{env} . The adiabatic index in the envelope, γ_{env} , ranges between the isentropic value, $\gamma_{\text{env}} = \gamma_{p,\text{env}} = 2/3$, and $\gamma_{\text{env}} = \gamma_\infty = 1$, while γ_{core} is confined to the corresponding range for the isothermal core (§4.3). Note the qualitative similarity between Fig. 9b and Figs. 4a and b.

Since the CPS has one more free parameter than the CIS, it is interesting to examine properties of the critical state as n varies. In Figure 10a, we plot $(\rho_c/\rho_s)_{\text{cr}}^{\text{max}}$ and $(P_c/P_s)_{\text{cr}}^{\text{max}}$ versus $\gamma_{p,\text{env}} = 1 + 1/n$ for $\tau_i = 1, 2, 3$, and 5. Here, we fix $\gamma_{\text{core}} = 1.1$ and take $\gamma_{\text{env}} = \gamma_{p,\text{env}} + 0.15$, in order to focus on the variation with n . Because $\gamma_{\text{env}} = \gamma_{p,\text{env}} + 0.15$ and equation (36) have two points of intersection in the $(\gamma_{\text{env}}, \gamma_{p,\text{env}})$ plane, there are two distinct values of $\gamma_{p,\text{env}}$ where $(\rho_c/\rho_s)_{\text{cr}}^{\text{max}}$ and $(P_c/P_s)_{\text{cr}}^{\text{max}}$ become infinite: $\gamma_{p,\text{env}} = 0.22$ and 1.18. The $\gamma_{p,\text{env}}$ at which $(\rho_c/\rho_s)_{\text{cr}}^{\text{max}}$ is a minimum is roughly insensitive to τ_i ; it lies in the range $0.75 \lesssim \gamma_{p,\text{env}} \lesssim 0.90$ ($-10 \lesssim n \lesssim -4$) for $\tau_i \leq 3$.

As in the case of the non-isentropic CIS, critical masses well in excess of the Bonnor-Ebert mass of the core may obtain for

the non-isentropic CPS, *even when* $\tau_i = 1$. This divergence of the mass is associated with a divergence of $c_s^3/\rho_s^{1/2}$; if the properties of the surface are known, then of course there is no divergence (§3). This behavior is illustrated in Fig. 10b, which shows the maximum critical mass (once again, obtained from the run of $m_{\text{CPS,cr}}$ versus r_i/r_s) for CPSs of different τ_i , as a function of $\gamma_{p,\text{env}}$ (solid curves). As above, we fix $\gamma_{\text{core}} = 1.1$. The dotted curve is for isentropic pure polytropes, for which $m_{p,\text{cr}}$ is always finite. The dashed curves correspond to pure polytropes for the same values of τ_i , that is, having central temperatures $T_c = \tau_i T_{\text{core}}$. Notice how the CPS mass is always equal to or greater than the pure polytropic mass. Also, the former greatly exceeds the latter at low values of $\gamma_{p,\text{env}}$, diverging more quickly than the pure polytrope for all values of τ_i . Conversely, at large $\gamma_{p,\text{env}}$ the effect of the isothermal core is clearly seen, as $m_{\text{CPS,cr}}^{\text{max}}$ remains finite; by contrast, $m_{p,\text{cr}}$ rapidly approaches zero as $\gamma_{p,\text{env}} \rightarrow 6/5$ and γ exceeds $4/3$ (MH). The limiting mass as $\gamma_{p,\text{env}} \rightarrow 6/5$ is slightly less than m_{BE} simply because $\gamma_{\text{core}} > \gamma_{p,\text{core}} = 1$ (§4.3).

5.5. Mean Quantities in the CIS and CPS

The existence of large pressure contrasts in the CIS and CPS does not necessarily imply that their *mean* pressures are also larger than the Bonnor-Ebert value. In fact, this is possible only for non-isentropic models. The mean pressure is given by

$$\bar{P} = \langle c^2 \rangle \bar{\rho},$$

where

$$\langle c^2 \rangle = \frac{\int_0^{r_s} r^2 \rho c^2 dr}{\int_0^{r_s} r^2 \rho dr}$$

is the mass-average of the squared sound speed, and $\bar{\rho} = M(r_s)/(4\pi r_s^3/3)$ is the mean density. We have calculated the mean-to-surface pressure ratio, \bar{P}/P_s , for a range of models, with the following results: (i) \bar{P}/P_s of the critical isentropic CIS or CPS is always less than or equal to the Bonnor-Ebert value, $(\bar{P}/P_s)_{\text{BE}} = 2.43$. (ii) The non-isentropic CIS has $\bar{P}/P_s > (\bar{P}/P_s)_{\text{BE}}$ for all r_i/r_s , as shown in Figure 11a. If $\gamma_{\text{core}} > \gamma_{\text{env}}$, then the maximum \bar{P}/P_s is obtained in the pure core limit, and vice-versa for $\gamma_{\text{env}} > \gamma_{\text{core}}$. Since the upper bound is for a single component isothermal sphere, we can use the results of MH to set an upper limit of $\bar{P}/P_s \leq 3.78$. (iii) The non-isentropic CPS has \bar{P}/P_s less than the corresponding non-isentropic CIS. When the core size is significant ($r_i/r_s \gtrsim 0.2$, as shown in Fig. 11b for $n = -3$), the pressure ratio can substantially exceed $(\bar{P}/P_s)_{\text{BE}}$; otherwise, $\bar{P}/P_s \simeq (\bar{P}/P_s)_{\text{NIP}} < (\bar{P}/P_s)_{\text{BE}}$. The last result follows from the fact that \bar{P}/P_s is not greatly enhanced for non-isentropic versus isentropic NIPs, even as $\gamma \rightarrow \gamma_\infty$. As shown by MH,

$$\left(\frac{\bar{P}}{P_s}\right)_{\text{NIP}} \leq 1.26 \frac{3(2-\gamma_p)}{(6-5\gamma_p)} = 1.26 \frac{3(n-1)}{(n-5)},$$

so that $(\bar{P}/P_s)_{\text{max}} = 1.89$ and 3.78 for $n = -3$ and $n = -\infty$, respectively. These limits are consistent with the limiting values shown in Fig. 11b.

5.6. Summary—CPS

The results of this section lead to two general conclusions concerning the approximation of mean and fluctuating magnetic fields by isotropic pressure components (see also MH).

First, both the maximum dimensionless mass m_{CP} that can be supported in a given model and the maximum pressure contrast are determined by the values of the polytropic *and* adiabatic indexes. As $\gamma - \gamma_p$ ($\gamma < 4/3$) increases in either the core or the envelope, $(P_c/P_s)_{CP,cr}$ becomes orders of magnitude larger than its isentropic value. This behavior qualitatively mimics that found in equilibrium calculations of magnetized isothermal clouds, which feature stable pressure contrasts well in excess of the Bonnor-Ebert value for strong magnetic fields (Mouschovias 1976; Tomisaka et al 1988). However, the behavior of the ratio of the *mean* pressure to that at the surface is quite different: we have extended the results of MH to composite polytropes with negative-index envelopes and shown that $\bar{P}/P_s < 4$, just as in the case of single component NIPs.

Second, the restriction to isentropic NIPs, whether single-component or composite with $\tau_i \simeq 1$, puts severe limitations on the mass range of the resulting models. Equilibrium clouds of mass substantially larger than the Bonnor-Ebert mass of the core do not exist under these restrictions. On the other hand, in the more likely case of non-isentropic polytropes ($\gamma_{env} > \gamma_{p,env}$ due to the presence of a mean magnetic field and Alfvén waves), both single-component NIPs and composite CPSs can have much larger critical masses.

The distinction between isentropic and non-isentropic polytropes is best seen by putting the critical mass in dimensional form. The mass of a composite polytrope is

$$M_{CP} = \frac{c_{core}^4}{P_s^{1/2} G^{3/2}} m_{CP} = 2.2 M_\odot \left(\frac{T_{core}}{10 \text{ K}} \right)^2 \times \left(\frac{2 \times 10^4 \text{ cm}^{-3} \text{ K}}{P_s/k} \right)^{1/2} m_{CP}, \quad (37)$$

Thus $2.6 M_\odot \leq M_{CP} \leq 3.6 \tau_s^2 M_\odot$, assuming these representative values (see eq 35). The larger upper limit, compared to the CIS (34), is due to the increased mass for pure $n = -2.9$ polytropes when expressed in terms of the central temperature. For a given surface temperature and pressure, $M_{CP,cr} \leq 3.6 \tau_s^2 M_\odot$ depends only weakly on whether the polytropic envelope is isentropic or not. However, the core temperature is rarely less than about 10 K; for a fixed core temperature and surface pressure, the maximum critical mass scales as $\tau_s^2 \propto (P_c/P_s)^{-2(1-1/\gamma_p)}$, which is limited for isentropic NIPs, but can be unbounded for non-isentropic ones. This fact has important consequences for the observed structure of embedded dense cores, a topic we take up in the following section.

Although the composite polytropes discussed in this paper represent the simplest possible improvement on pure polytropic models, they already suggest a number of interesting implications for star formation generally. We discuss a few of these below.

6. DISCUSSION

6.1. Near-Critical Cores with Massive Envelopes

An interesting consequence of our results for the non-isentropic CPS (§5.4) is the existence of equilibria featuring massive envelopes surrounding approximately Bonnor-Ebert mass cores, a property reminiscent of the observations reviewed in §1.2. Since the derived mass ratio of ^{13}CO envelopes to NH_3 cores is of order 10–100, we choose an example CPS which illustrates this mass range.

⁸Recall that $m > m_{cr}$ for non-isentropic states with $(P_c/P_s)_{BE} < P_c/P_i < (P_c/P_i)_{cr}$ (Fig. 1).

The core, envelope, and total dimensionless masses of a $n = -3$ CPS with $\gamma_{core} = 1.2$, $\gamma_{env} = 0.94$ are displayed as a function of the core fraction r_i/r_s in Figure 12a. The critical mass of the core alone, $m_{core,cr}$, has also been plotted, in the same non-dimensionalization. For a fixed central sound speed c_{core} and outer surface pressure P_s , the pressure on the core, P_i , increases as the core fraction shrinks; hence, $m_{core,cr} \propto M_{core,cr} \propto P_i^{-1/2}$ decreases with decreasing r_i/r_s . Fig. 12a has a very interesting property: the mass of the core remains very near (and indeed, somewhat exceeds⁸) its critical mass for $r_i/r_s > 1.3 \times 10^{-2}$, despite the fact that the corresponding mass of the envelope varies by more than an order of magnitude over the same range. If observed in a high-density tracer, such a core would appear to have a virial parameter of nearly the Bonnor-Ebert value ($\alpha = 2.06$; Bertoldi & McKee 1992), as is observed. In terms of our dimensionless variables, the virial parameter becomes (see §1.2)

$$\alpha = \frac{5 \langle \sigma^2 \rangle \bar{R}}{GM} = \left(4\pi \frac{P_c}{P_s} \right)^{1/2} \frac{5 \langle \sigma^2 \rangle \bar{\xi}}{m \sigma_{th}^2}.$$

Taking $\langle \sigma^2 \rangle = \sigma_{th}^2$, $\bar{\xi} = \xi_i$, and $m = m_{core}$, we find $\alpha_{core} \simeq 2$ for all $r_i/r_s > 1.3 \times 10^{-2}$, as shown by the upper curve in Fig. 12b. It is of interest to compare α_{core} with the virial parameter for the entire cloud, α_{tot} . We estimated the mean velocity dispersion of the latter using equation (22), and by assuming $\langle \sigma^2 \rangle \gg \sigma_{th}^2$ (valid for $r_i \ll r_s$) and an Alfvén Mach number of 1, i.e. $v_A^2 = 3 \langle \sigma^2 \rangle$ (Myers & Goodman 1988; Crutcher 1999). This gives $\langle \sigma^2 \rangle \simeq c^2/3$. Strictly speaking, the latter should change with r_i/r_s , but this estimate suffices to get a rough idea of the magnitude of α_{tot} . Finally, taking $\bar{\xi} = \xi_s$ and $m = m_{CP}$, we find that α_{tot} varies between 0.73 and 1.5 as r_i/r_s ranges from 0 to 1 (Fig. 12b). Values of $\alpha_{tot} < 1$ simply reflect the limited validity of our estimated $\langle \sigma^2 \rangle$ —as $r_i \rightarrow r_s$, the cloud becomes thermally dominated with $\langle \sigma^2 \rangle \rightarrow c^2$, not $c^2/3$ as we have assumed.

Insofar as the derived virial parameters of many clumps on sub-GMC scales are much greater than unity (§1.2), we conclude (with Bertoldi & McKee 1992), that such clumps are pressure-confined. Sub-critical CPSs having $M_{env} = 10 - 100 M_{core}$ are easily constructed. In our view, these results present a reasonable explanation for why it is that PPCs, which are nearly critical by virial theorem estimates (§1.2), can exist within clumps and GMCs that are far more massive but nonetheless stable or close to critical. This constitutes an explicit realization of the formalism developed by Bonazzola et al (1987), who proposed that a turbulent cloud could be stable on large scales and unstable on small ones (note that our models are stable by construction, but would become unstable if the core mass were increased further for $r_i/r_s > 1.3 \times 10^{-2}$). A more detailed comparison of this aspect of the models with existing data is, however, beyond the scope of this paper.

6.2. The Formation of Very Low-Mass Stars

The enhanced pressure contrasts attainable in the composite models may also have implications for forming very low-mass stars such as brown dwarfs. A simple argument for an isolated core forming a single star serves to illustrate this point. In order to form a star of mass M_* , it is necessary to collect together at least a Bonnor-Ebert mass, $M_{BE} = 2.6 (T/10 \text{ K})^2 [P_s/(2 \times 10^4 \text{ k}_B) \text{ K cm}^{-3}]^{-1/2} M_\odot$, of gas. Observed cores in GMCs

have surface pressures ranging from $P_s/k_B \sim 4 \times 10^4$ (Taurus, Cepheus) to 3×10^5 K cm³ (Orion) (Solomon et al 1987; Bertoldi & McKee 1992), so it is easy to form stars with $M_* \simeq 0.7 - 1.8 M_\odot$. But to create a star of much smaller mass (brown dwarfs have $M_* \lesssim 0.08 M_\odot$), it is necessary to either reduce the temperature below 10 K (which is difficult due to radiative trapping— de Jong et al 1980), or to increase P_s/k_B well beyond the observed range. Inserting $M_J \lesssim 0.08 M_\odot$ into the above, one finds $P_s/k_B \gtrsim 1.3 \times 10^8$ K cm³, nearly three orders of magnitude above the observed pressures. In a CPS with $m_{\text{core}} = 0.08 M_\odot$, however, it is the pressure on the core-envelope interface, P_i , that counts. Here one is not limited by the Bonnor-Ebert value $P_i/P_s = 14.04$, since the pressure drop through a non-isentropic envelope can be much larger (Fig. 10a). Thus, non-isentropic CPSs lead to the possibility of a structure near the brink of instability with a core small enough to make a brown dwarf. Whether it is possible for the core to undergo collapse without having a significant mass from the envelope fall on it, thereby increasing its mass, cannot be determined from hydrostatic calculations such as ours.

6.3. Protostellar Collapse

One of the more robust predictions of studies of cloud collapse is the mass accretion rate onto the nascent central object. The well-studied SIS, for example, features a time-independent accretion rate, $\dot{M}_{\text{SIS}} = 0.975 \sigma_{\text{th}}^3 / G$ (Shu 1977). Observational estimates of \dot{M} have been inferred for many Class 0 and Class I infrared sources, from the peak of their spectral energy distributions in the far-infrared (Hartmann 1998). These fall within the range $1.6 \times 10^{-6} M_\odot \text{ yr}^{-1}$ (Class I) $\lesssim \dot{M} \lesssim 10^{-4} M_\odot \text{ yr}^{-1}$ (Class 0). For a typical $\sigma_{\text{th}} \sim 0.2 \text{ km s}^{-1}$, the SIS is in accord with the lower limit of this range, but is inconsistent with the high \dot{M} 's of the Class 0 objects. This again raises the question of the relevance of the SIS for the earliest stages of protostellar evolution (Foster & Chevalier 1993; Safier et al 1997).

We now attempt to predict how the collapse of a composite polytrope will differ from that of previous models. Since we have modeled the core of a CPS with an isothermal sphere, the early behavior is likely to be similar to that of the Bonnor-Ebert sphere, which was investigated most recently by Foster & Chevalier (1993). They found that \dot{M} is largest at the onset of collapse, then decreases, eventually approaching \dot{M}_{SIS} . The late-time behavior is more uncertain, and depends on the characteristics of the envelope. If the envelope can be described by a NIP, then two recent studies suggest that the accretion rate will increase at late times: McLaughlin & Pudritz (1997) considered expansion wave solutions in singular polytropic spheres and found that $\dot{M} \propto t^{-3/n}$ ($n < -1$); i.e., the accretion rate is small at early times, then increases monotonically. Henriksen, André, & Bontemps (1997) studied the collapse of a pressureless model (so that there is no expansion wave) with a piecewise continuous density profile: $\rho \propto r^0$ in the core and $\rho \propto r^{-2n/(n-1)}$ (corresponding to a singular polytropic sphere) in the envelope. Their results show that after an initial burst of accretion (\dot{M} is formally infinite in their model, due to the pressureless, flat inner region), models with $n < -1$ pass through a minimum in \dot{M} ($> \dot{M}_{\text{SIS}}$), before increasing monotonically at large t as $t^{-3/n}$, in agreement with the results of McLaughlin & Pudritz. On the other hand, if the envelope is supported by a static magnetic field so that the late-time accretion is regulated by ambipolar diffusion, the accretion rate is similar to that of an SIS (Safier et al 1997). More definitive results for the collapse of a CPS

await detailed numerical calculations.

7. SUMMARY

In this paper, we have developed a polytropic theory of molecular clouds that improves on previous work in several ways. The consideration of spatially separate core and envelope regions is in better accord with the known velocity structure of star-forming cloud cores. Such an approach allows a thermally-dominated core to coexist with a nonthermally-dominated envelope in a single, self-gravitating equilibrium structure. In the formalism developed here, the core and the envelope are each represented by a single pressure component with properties chosen to approximate the combined effects of thermal pressure and static magnetic fields in the core (assumed to be described by a polytropic index $\gamma_p = 1$), and these plus turbulent motions in the envelope. The results for isothermal envelopes are summarized in §4.4, and those for polytropic envelopes in §5.6. Just as composite polytropic models of stars were created to reflect changing physical conditions with radial scale, cloud models can now do the same. Our models are non-singular, a feature in better concord with observations of the densest pre-protostellar cores than the singular hypothesis. This agreement carries over to the quantitative comparison of both the density and velocity dispersion profiles with those observed, as we present in detail in a subsequent paper.

The increase of temperature near the surface and of line width with size had led previous workers to consider negative-index polytropes (NIPs) as models of interstellar clouds (Shu et al 1972; Maloney 1988). In general, these models were based on the assumption that the gas is isentropic—i.e., that the polytropic index γ_p is the same as the adiabatic index γ . The maximum pressure and density drops in such NIPs are always less than that of a Bonnor-Ebert sphere, however, suggesting that they are inadequate as models for molecular clouds. Isentropic composite polytropes of reasonable core fractions already provide pressure and density enhancements well in excess of those of the isothermal sphere. The critical mass and radius of an isentropic composite polytropic sphere (CPS) can also exceed the Bonnor-Ebert mass of the core in cases where the kinetic temperature of the envelope is higher than that of the core.

However, the pressure components in molecular gas, particularly magnetic fields and turbulence (which we model with Alfvén waves), are *not* isentropic (MH). Non-isentropic CPSs permit pressure and density drops in stable structures that are as large as those observed, and in addition permit masses that can be large compared with the Bonnor-Ebert mass of the core, even without a temperature difference between core and envelope. However, as found by MH for individual NIPs, the ratio of the *mean* pressure to the surface pressure for composite polytropes with negative-index envelopes must be less than a factor ~ 4 , which appears to be a general feature of hydrostatic models for self-gravitating clouds with outwardly increasing temperatures. The greater flexibility of the CPS allows one to transcend the limitations of many previous polytropic models, which were unable to reproduce even the bulk physical properties of PPCs, not to mention the detailed spatial structure of these quantities.

The authors would like to thank Dean McLaughlin for useful discussions. This research is supported in part by a NASA grant to the Center for Star Formation Studies. The research of CC was supported in part by an NSERC Postdoctoral Fellowship. The research of CFM is supported in part by a grant from the NSF (AST95-30480), a Guggenheim Fellowship, and

a grant from the Sloan Foundation to the Institute for Advanced Study. CC thanks the Astronomy Group at the University of Western Ontario for their hospitality while this work was completed. CFM wishes to express his appreciation to John Bahcall of the Institute for Advanced Study and Edith Falgarone of the Ecole Normale Supérieure for their hospitality.

APPENDIX

ON THE STABILITY CRITERION FOR POLYTROPIC MODELS OF MOLECULAR CLOUDS

As discussed in §1.4, the stability analysis of bounded polytropes has been pursued in the literature according to two very different assumptions about the response of the cloud to small perturbations. Some authors have assumed that the central temperature remains constant during the perturbation, whereas we (in agreement with MH) have assumed that the entropy remains constant. For an isothermal gas, the two assumptions are equivalent; but in general they are not. The issue is not one of mere formalism: whether a given model is stable or not is highly sensitive to the choice.

The constant central temperature condition was justified by Maloney (1988) on the basis of the "... general uniformity of gas temperatures observed in molecular clouds over a large range of spatial and density scales ...". As Turner et al (1992) pointed out, however, it is the value of T_c for a *given* cloud *during* a perturbation that is relevant to the issue of stability. Still asserting the constancy of T_c , however, the latter authors argued that it "... is determined by the cloud's extinction and the local UV [field], and variations in $[T_c]$ due to (small) variations in [the boundary pressure] may reasonably be considered negligible."

The issue becomes more involved when we consider that these authors view the increasing outward temperature of NIPs as being partly or entirely *nonthermal* in origin. In the models of both Maloney and McLaughlin & Pudritz (1996), e.g., the kinetic temperature is spatially constant (and supposed equal to T_c), but superposed on this is an isotropic, turbulent velocity field $\delta\mathbf{v}$, whose *effective* temperature, $T_{\text{eff}} \propto \langle \delta\mathbf{v} \rangle^2$, behaves like that of a NIP. This is, in fact, in accord with recent observations of Bok globules showing that the gas temperature throughout a given globule is remarkably uniform, even though the non-thermal linewidth can be up to twice the thermal value (Lemme et al 1996). The origin of the turbulent motions producing the nonthermal linewidths is the object of much speculation (e.g. Alfvén waves, cloud-cloud motions, protostellar outflows, etc.), but it is certainly different than the mechanisms that determine the thermal motions in the gas.

In a polytropic model, the surface temperature is related to the central temperature by

$$\frac{T_s}{T_c} = \left(\frac{P_c}{P_s} \right)^{1/(n+1)} = \left(\frac{P_c}{P_s} \right)^{(1-\gamma_p)/\gamma_p}. \quad (38)$$

The central region is often sufficiently shielded that the temperature there is determined by cosmic ray heating. Thus, while it is plausible that T_c remains constant during the perturbation, there is no justification for assuming that T_s , which is represented in the turbulent models by the velocity dispersion at the surface of the cloud, will change just so as to satisfy this relation with $T_c = \text{const}$. Indeed, there is no known relation between the physical processes determining the kinetic temperature and the

nonthermal velocity dispersion *anywhere in the cloud*. Furthermore, as pointed out by MH, both Maloney and McLaughlin & Pudritz considered isentropic polytropes. Such polytropes cool upon compression if $\gamma_p < 1$, as they assumed. In order to maintain a constant central temperature, energy would have to be supplied, and no plausible energy source has been identified. In the language of §2.1 and MH, the isothermal perturbations considered by these authors are neither locally nor globally adiabatic, since heat is not simply redistributed but rather is injected by some unknown agent.

In our analysis, we avoid these contradictions and follow most previous authors by taking the perturbations to be locally adiabatic (§2.1): no heat enters or leaves the system (cf. Shu et al. 1972; Viala & Horedt 1974; Stahler 1983). However, we depart from these treatments by allowing for *non-isentropic* pressure components, whose adiabatic index γ , which dictates the stability properties of the gas, differs from the polytropic index γ_p [or $n = 1/(1 - \gamma_p)$], which determines the equilibrium structure. For NIPs in particular, taking $\gamma > \gamma_p$ moves the critical point of equilibrium to larger dimensionless radii, and more centrally condensed states (Fig. 1), than in the isentropic ($\gamma = \gamma_p$) case. These newly-accessible equilibria are identical to those *assumed* to exist by the above authors, but are not derived from the questionable assumption of unnamed energy sources.

REFERENCES

- André, P., Ward-Thompson, D., & Motte, F. 1996, *A&A*, 314, 625
 Bachiller, R., & Cernicharo, J. 1984, *A&A*, 140, 414
 Bachiller, R., Guilloteau, S., & Kahane, C. 1987, *A&A*, 173, 324
 Beech, M. 1988, *ApSS*, 146, 299
 Beichman, C.A., Myers, P.C., Emerson, J.P., Harris, S., Mathieu, R., Benson, P.J., & Jennings, R.E. 1986, *ApJ*, 307, 337
 Benson, P.J., & Myers, P.C. 1989, *ApJS*, 71, 89
 Bertoldi, F., & McKee, C.F. 1992, 395, 140
 Boland, W., & de Jong, T. 1984, *A&A*, 134, 87
 Bonazzola, S., Falgarone, E., Hayvaerts, J., Perault, M., & Puget, J.L. 1987, *A&A*, 172, 293
 Bonnell, I.A., Bate, M.R., & Price, N.M. 1996, *MNRAS*, 279, 121
 Bonnor, W.B. 1956, *MNRAS*, 116, 350
 Boulares, A., & Cox, D.P. 1990, *ApJ*, 365, 544
 Bourke, T.L., Hyland, A.R., Robinson, G., James, S.D., Wright, C.M. 1995, *MNRAS*, 276, 1067
 Casali, M.M. 1986, *MNRAS*, 223, 341
 Caselli, P., & Myers, P.C. 1995, *ApJ*, 446, 665
 Caselli, P., Walmsley, C.M., Terzieva, R., & Herbst, E. 1998, *ApJ*, 499, 234
 Cernicharo, J., Bachiller, R., & Duvert, G. 1985, *A&A*, 149, 273
 Chandrasekhar, S. 1939, *An Introduction to the Study of Stellar Structure* (New York: Dover)
 Chandrasekhar, S., & Wares, G.W. 1949, *ApJ*, 109, 551
 Clemens, D.P., & Barvainis, R. 1988, *ApJS*, 68, 257
 Clemens, D.P., Yun, J.L., & Heyer, M.H. 1991, *ApJS*, 75, 877
 Cowling, T.G. 1941, *MNRAS*, 101, 367
 Crutcher, R.M. 1999, *ApJ*, 520, 706
 de Jong, T., Dalgarno, A., & Boland, W. 1980, *A&A*, 91, 68
 Dickman, R.L., & Clemens, D.P. 1983, *ApJ*, 271, 143
 Ebert, R. 1955, *ZAp*, 37, 216
 Eddington, A.S. 1926, *The Internal Constitution of the Stars* (Cambridge: Cambridge University Press)
 Elmegreen, B.G. 1989, *ApJ*, 338, 178
 Falgarone, E., & Puget, J.L. 1985, *A&A*, 142, 157
 Foster, P.N., & Chevalier, R.A. 1993, *ApJ*, 416, 303
 Fuller, G.A. 1989, PhD Thesis, University of California at Berkeley
 Fuller, G.A., & Myers, P.C. 1992, *ApJ*, 384, 523
 Gaida, M., Ungerechts, H., & Winnewisser, G. 1984, *A&A*, 137, 17
 Gehman, C.S., Adams, F.C., Fatuzzo, M., & Watkins, R. 1996, *ApJ*, 457, 718
 Genzel, R. 1992, in *The Galactic Interstellar Medium*, Saas-Fee Advanced Course 21, Lecture Notes 1991, ed. D. Pfenniger & P. Bartholdi (Berlin: Springer-Verlag), p. 295
 Goodman, A.A., Barranco, J.A., Wilner, D.J., & Heyer, M.H. 1998, *ApJ*, 504, 223
 Hartmann, L. 1998, *Accretion Processes in Star Formation* (Cambridge: Cambridge University Press), §4
 Hasegawa, T.I. 1988, *PASJ*, 40, 219
 Henrich, L.R., & Chandrasekhar, S. 1941, *ApJ*, 94, 525
 Henriksen, R., André, P., & Bontemps, S. 1997, *A&A*, 323, 549
 Holliman, J.H. 1995, PhD Thesis, University of California at Berkeley
 Hunter, C. 1977, *ApJ*, 218, 834
 Kulsrud, R.M., & Pearce, W.P. 1969, *ApJ*, 156, 445
 Larson, R.B. 1981, *MNRAS*, 194, 809
 Ledoux, P., & Walraven, T. 1958, *Handbuch der Physik*, 51, 353 (Berlin: Springer)
 Lehtinen, K., Mattila, K., Schnur, G.F.O., Prusti, T. 1995, *A&A*, 295, 487
 Lemme, C., Wilson, T.L., Tieftrunk, A.R., & Henkel, C. 1996, *A&A* 312, 585
 Lizano, S., & Shu, F.H. 1989, *ApJ*, 342, 834
 Loren, R.B. 1989, *ApJ*, 338, 902
 Maloney, P. 1988, *ApJ*, 334, 761
 McKee, C.F., & Zweibel, E. 1995, *ApJ*, 440, 686
 McKee, C.F., & Holliman, J.H. 1999, *ApJ*, in press (MH)
 McKee, C.F., Zweibel, E.G., Goodman, A.A., & Heiles, C. 1993, in *Protostars and Planets III*, ed. E.H. Levy & J.I. Lunine (Tucson: University of Arizona Press), 327
 McLaughlin, D.E., & Pudritz, R.E. 1996, *ApJ*, 469, 194
 McLaughlin, D.E., & Pudritz, R.E. 1997, *ApJ*, 476, 750
 Mestel, L., & Spitzer, L. 1956, *MNRAS*, 116, 503
 Milne, E.A. 1930, *MNRAS*, 91, 4
 Milne, E.A. 1932, *MNRAS*, 92, 610
 Motte, F., André, P., & Neri, R. 1998, *A&A*, 336, 150
 Mouschovias, T.Ch. 1976, *ApJ*, 207, 141
 Mouschovias, T.Ch. 1991, in *The Physics of Star Formation and Early Stellar Evolution*, ed. C.J. Lada & N.D. Kylafis (Dordrecht: Kluwer), 449
 Myers, P.C., & Benson, P.J. 1983, *ApJ*, 266, 309
 Myers, P.C., & Fuller, G.A. 1992, *ApJ*, 396, 631
 Myers, P.C., & Goodman, A.A. 1988, *ApJ*, 326, L27
 Nelson, R.P., & Langer, W.D. 1997, *ApJ*, 482, 796
 Onishi, T., Mizuno, A., Kawamura, A., Ogawa, H., & Fukui, Y. 1996, *ApJ*, 465, 815
 Onishi, T., Mizuno, A., Kawamura, A., Ogawa, H., & Fukui, Y. 1998, *ApJ*, 502, 296
 Safier, P., McKee, C.F., & Stahler, S. 1997, *ApJ*, 485, 660
 Schönberg, M., & Chandrasekhar, S. 1942, 96, 161
 Shu, F.H. 1977, *ApJ*, 214, 488
 Shu, F.H., Adams, F.C., & Lizano, S. 1987, *Ann. Rev. Astron. Astrophys.*, 25, 23
 Shu, F.H., Milione, V., Gebel, W., Yuan, C., Goldsmith, D.W., & Roberts, W.W. 1972, *ApJ*, 173, 557
 Stahler, S.W. 1983, *ApJ*, 268, 165
 Stutzki, J., & Guesten, R. 1990, *ApJ*, 356, 513
 Stüwe, J.A. 1990, *A&A*, 237, 178
 Tomisaka, K., Ikeuchi, S., & Nakamura, T. 1988, *ApJ*, 335, 239
 Turner, B.E., Xu, L., & Rickard, L.J. 1992, *ApJ*, 391, 158
 Viala, Y.P., & Horedt, Gp. 1974, *A&A*, 33, 195
 Walén, C. 1944, *Arkiv mat. astron. fysik* 30A, No 15, 1
 Ward-Thompson, D., Scott, P.F., Hills, R.E., & André, P. 1994, *MNRAS*, 268, 276
 Williams, J.P., Blitz, L., & McKee, C.F. 1999, in *Protostars and Planets IV*, ed. V. Mannings, A. Boss, & S. Russell, University of Arizona Press, Tucson, in press
 Williams, J.P., Blitz, L., & Stark, A.A. 1995, *ApJ*, 451, 252
 Yabushita, S. 1968, *MNRAS*, 140, 109
 Yabushita, S. 1974, *MNRAS*, 167, 95
 Yabushita, S. 1975, *MNRAS*, 172, 441
 Young, J.S., Goldsmith, P.F., Langer, W.D., Wilson, R.W., & Carlson, E.R. 1982, *ApJ*, 261, 513
 Yun, J.L., & Clemens, D.P. 1990, *ApJ*, 365, L73
 Yun, J.L., & Clemens, D.P. 1991, *ApJ*, 381, 474
 Zweibel, E.G., & Josafatsson, K. 1983, *ApJ*, 270, 511

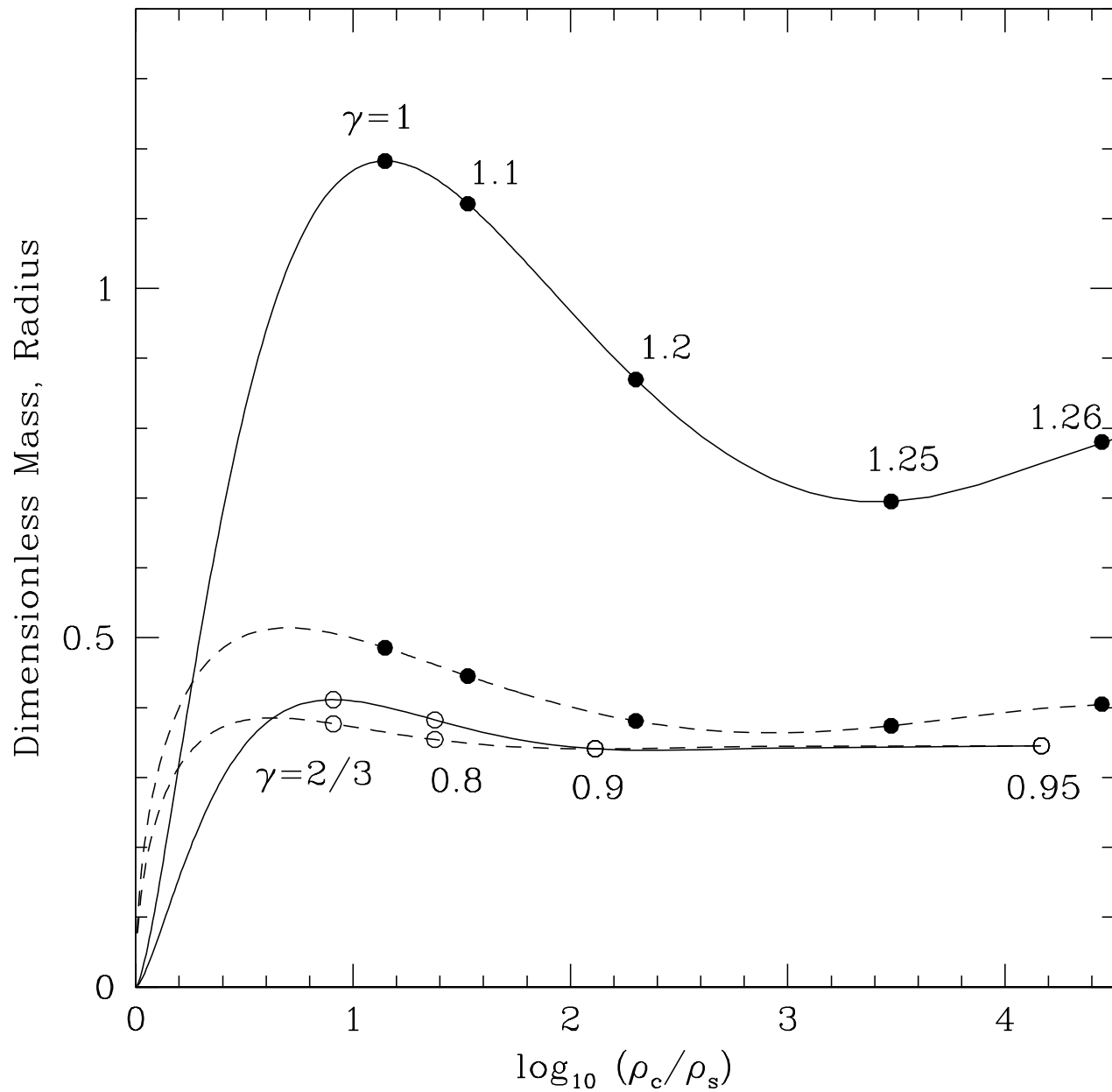


FIG. 1.— Equilibrium sequences of the isothermal sphere (curves with filled circles) and an $n = -3$ polytrope (curves with open circles). Solid lines show the dimensionless mass; dashed lines, the dimensionless radius. Dots indicate critical points at particular values of γ , as labeled.

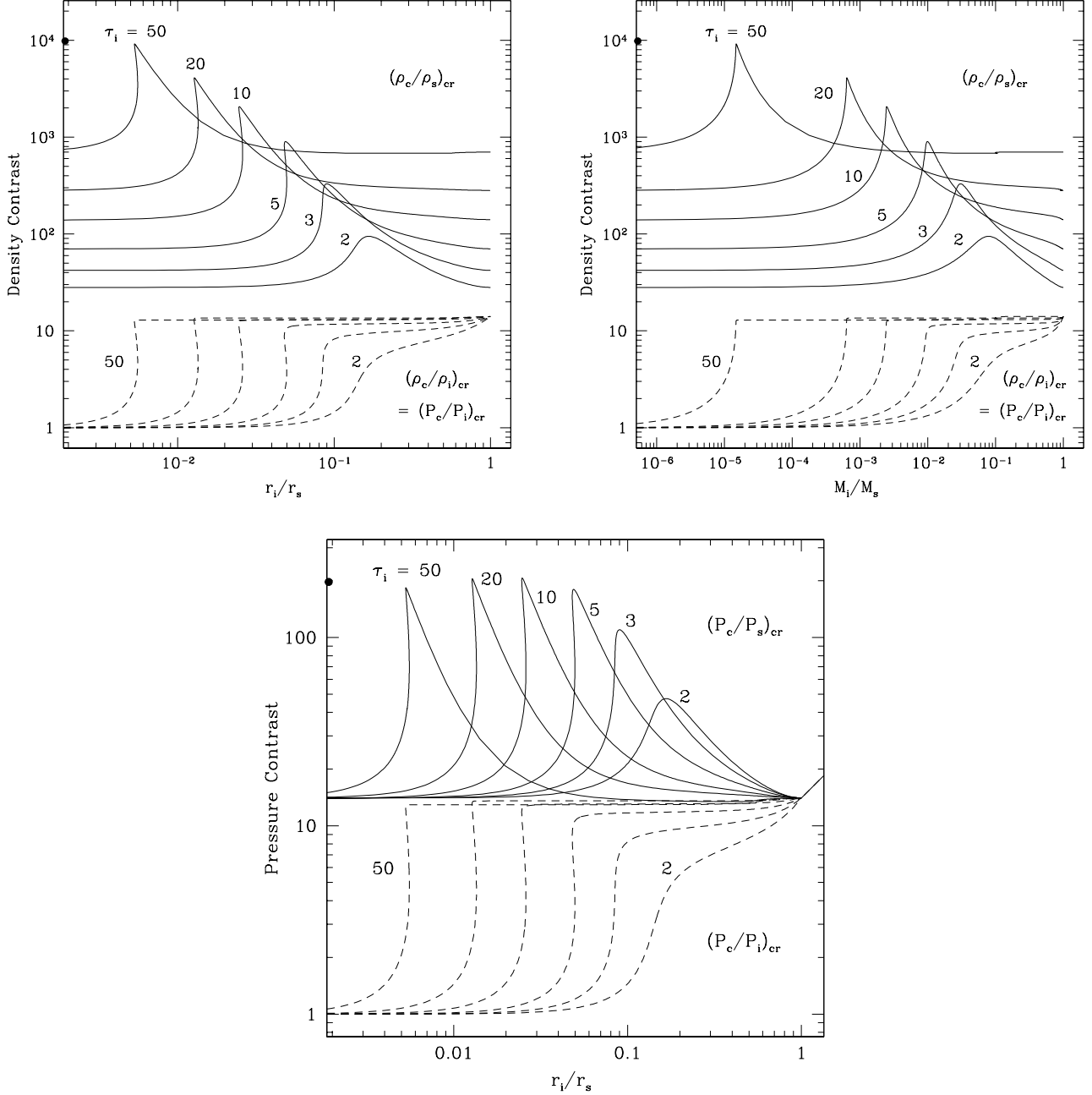


FIG. 2.— Density and pressure contrasts of the critically stable, isentropic CIS. (a) Critical density contrast as a function of fractional core radius, r_i/r_s . Each point on a curve represents a single, critically stable, equilibrium model. Solid curves are center-to-surface contrast, dashed curves center-to-core boundary contrast. Curves are labeled by values of τ_i . The filled circle on the ordinate indicates a density contrast of $\tau_i(\rho_c/\rho_s)_{BE}^2 = 50(14.04)^2 = 9855$. (b) Critical density contrast as a function of fractional core mass, using same notation as in (a). (c) Critical pressure contrast as a function of fractional core radius, using same notation as in (a). The filled circle on the ordinate indicates a pressure contrast of $(P_c/P_s)_{BE}^2 = (14.04)^2 = 197$.

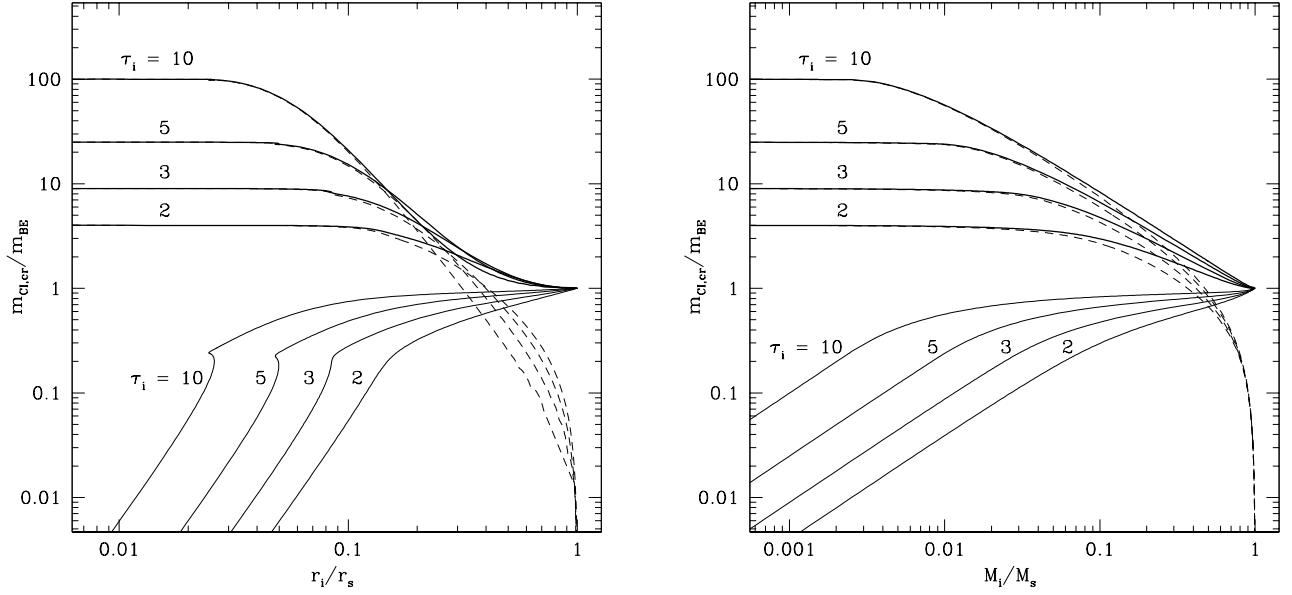


FIG. 3.— Dimensionless mass of the critically stable, isentropic CIS, normalized to the Bonnor-Ebert mass, $m_{\text{BE}} = 1.182$. (a) Critical mass as a function of fractional core radius, r_i/r_s . Solid curves show the core mass alone; dashed curves, the envelope mass; and the heavy solid curve the total of the two. Curves are labeled by values of τ_i . (b) Critical mass as a function of fractional core mass, using same notation as in (a).

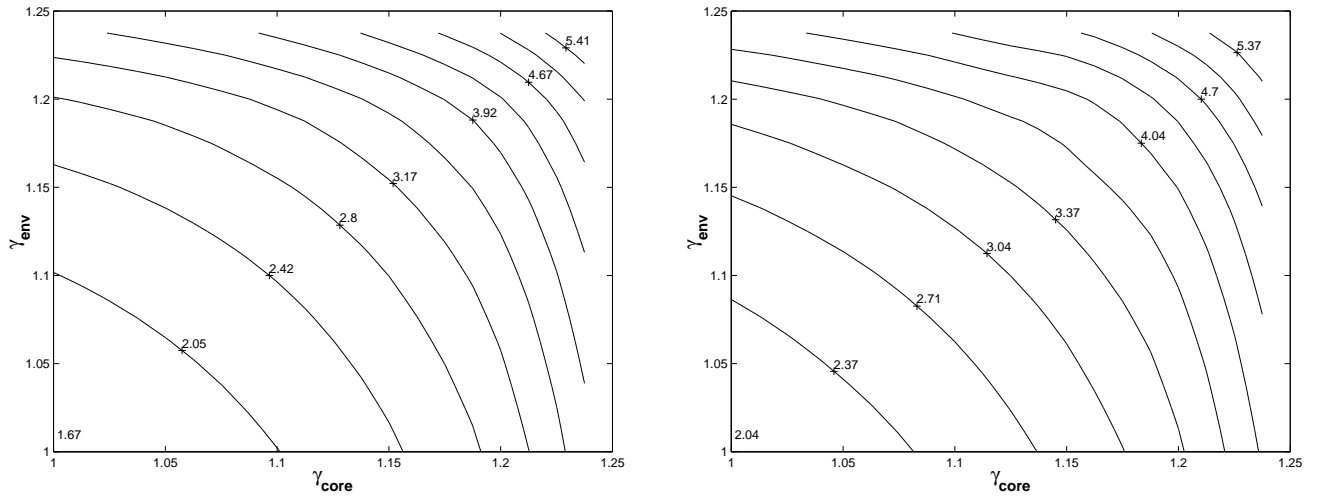


FIG. 4.— Maximum pressure contrast of the critically stable, non-isentropic CIS. Contours of equal $\log_{10}(P_c/P_s)_{\text{cr}}^{\text{max}}$ are plotted as a function of the core and envelope adiabatic indices, γ_{core} and γ_{env} , respectively, for (a) $\tau_i = 2$; (b) $\tau_i = 3$.

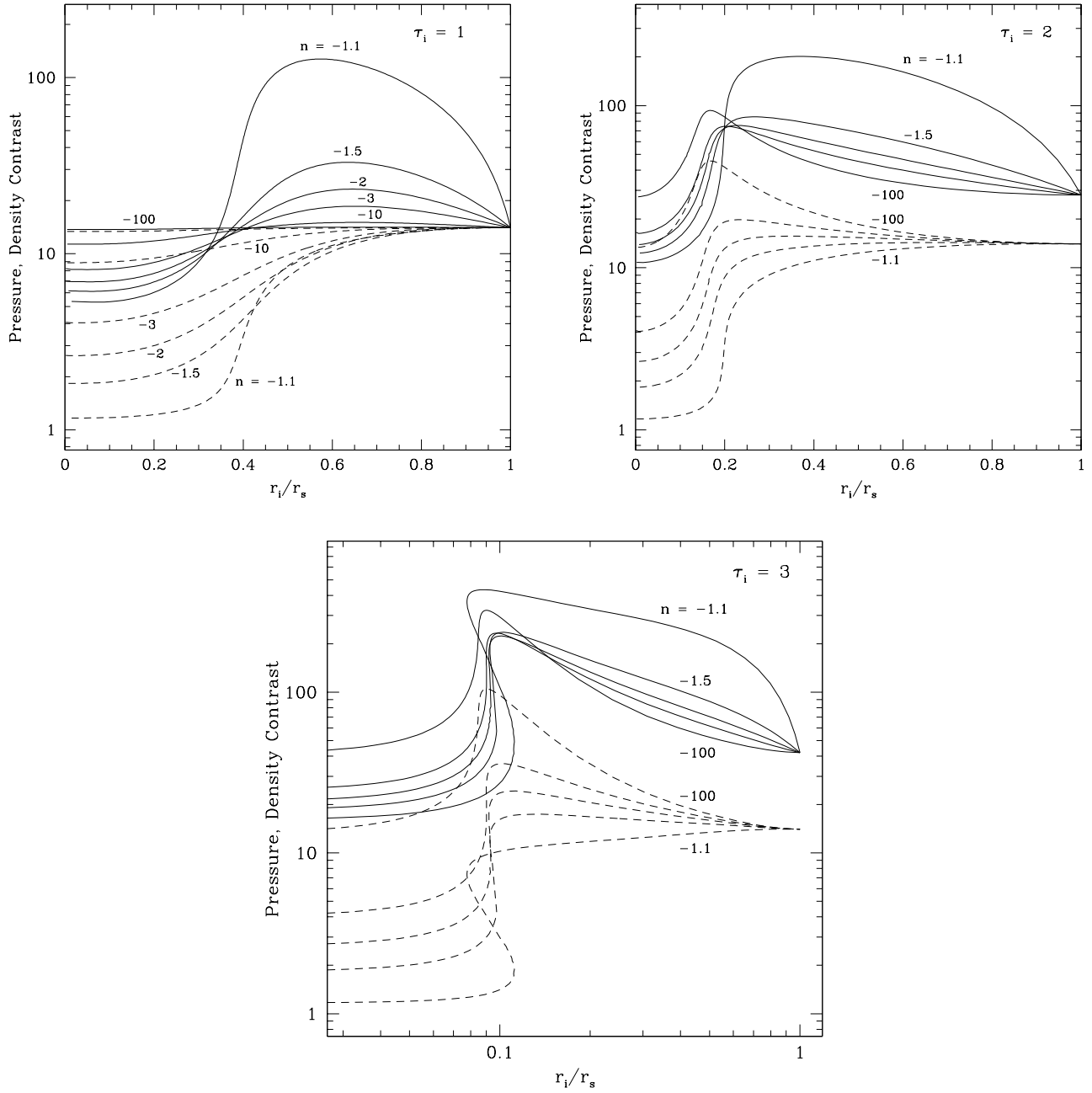


FIG. 5.— Pressure and density contrasts of the critically stable, isentropic CPS, in the cases (a) $\tau_i = 1$; (b) $\tau_i = 2$; and (c) $\tau_i = 3$. Solid curves show the center-to-surface density contrast; dashed curves, the center-to-surface pressure contrast. Both are plotted as a function of the fractional core radius. Curves are labeled by values of n .

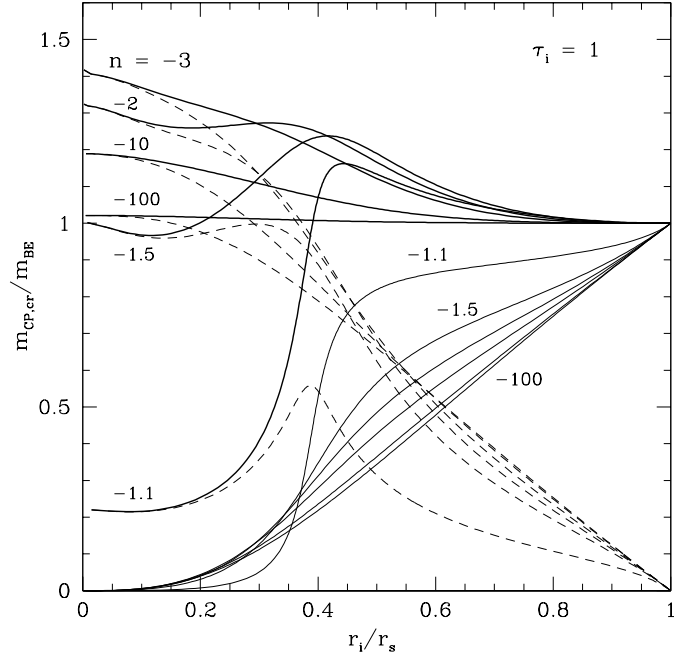


FIG. 6.— Dimensionless mass of the critically stable, isentropic CPS with $\tau_i = 1$, as a function of fractional core radius. Solid curves indicate the core mass, dashed curves the envelope mass, and heavy solid curves the sum of the two. Curves are labeled by values of n .

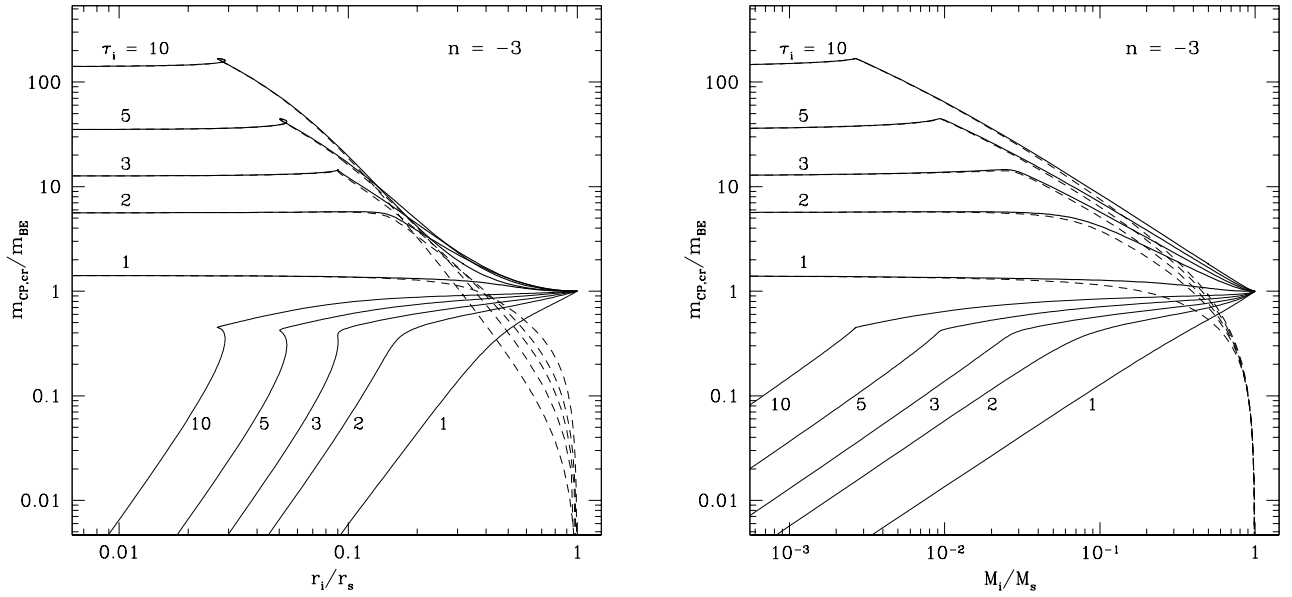


FIG. 7.— Dimensionless mass of the critically stable, isentropic CPS. (a) Critical mass, normalized to the Bonnor-Ebert mass m_{BE} , as a function of fractional core radius, r_i/r_s . Solid curves show the core mass alone; dashed curves, the envelope mass; and heavy solid curves the sum of the two. Curves are labeled by values of τ_i . (b) Critical mass as a function of fractional core mass, using same notation as in (a).

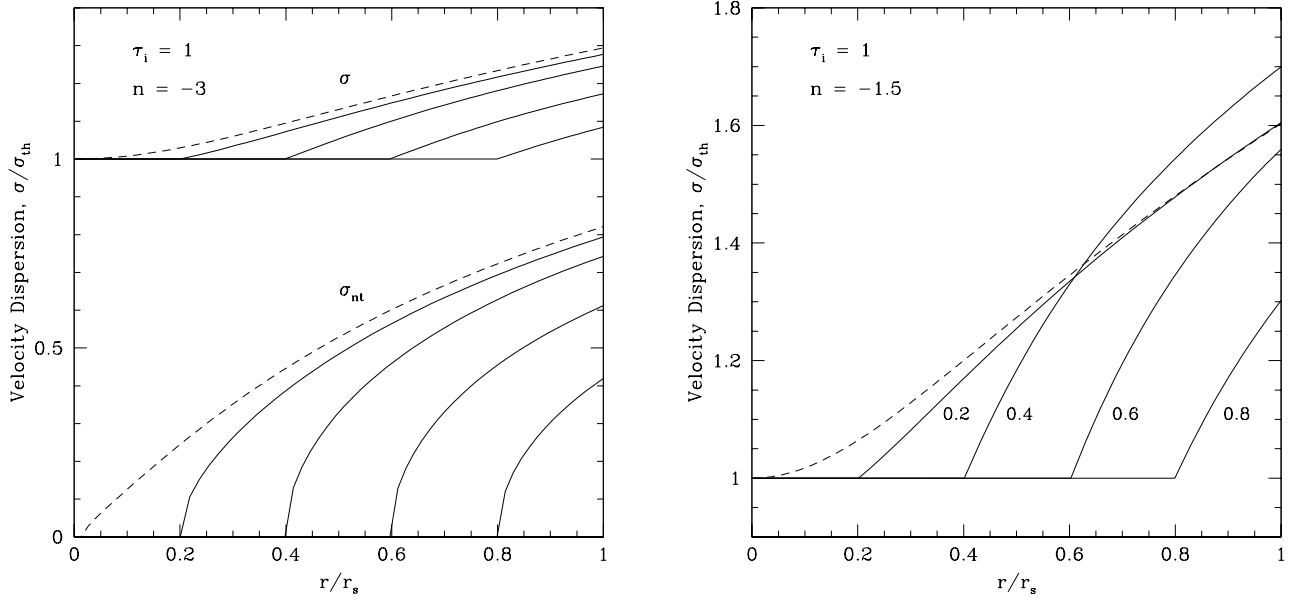


FIG. 8.— Velocity dispersion in the critically stable, isentropic CPS, assuming $v_A = 0$. (a) Total (top curves) and nonthermal (bottom curves) velocity dispersions for CPSs with $\tau_i = 1$, $n = -3$, and various values of r_i/r_s . From left to right: $r_i/r_s = 0.2, 0.4, 0.6$, and 0.8 . Also shown are the corresponding dispersion for a pure $n = -3$ polytrope (dashed curves). (b) Similar to (a), but for $n = -1.5$. Only the total dispersion is plotted.

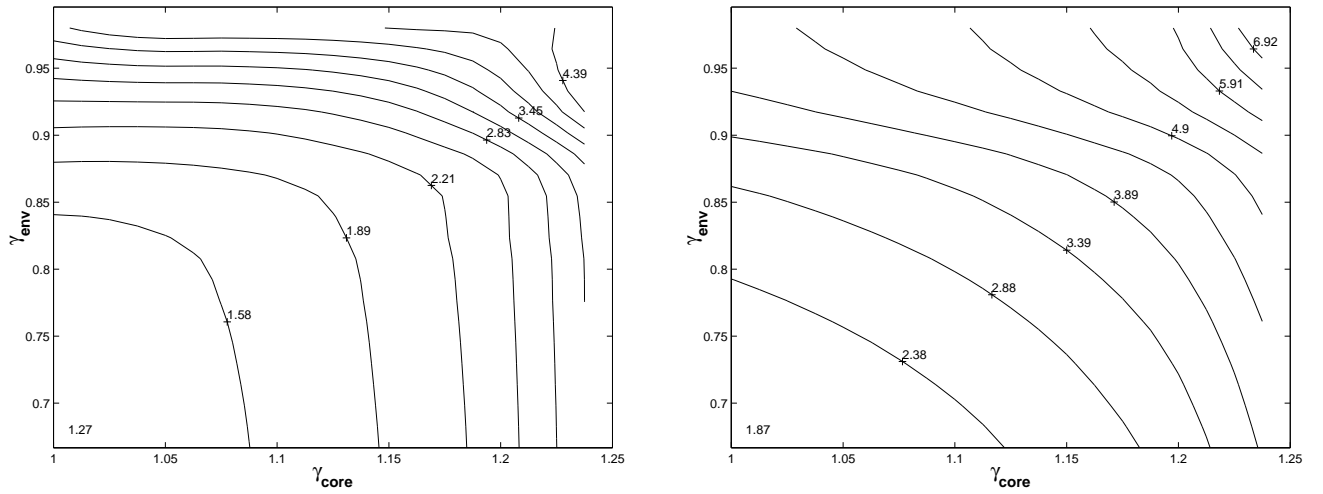


FIG. 9.— Maximum density contrast of the critically stable, $n = -3$ non-isentropic CPS. Contours of equal $\log_{10}(\rho_c/\rho_s)_{cr}^{max}$ are plotted as a function of the core and envelope adiabatic indices, γ_{core} and γ_{env} , respectively, for (a) $\tau_i = 1$; (b) $\tau_i = 2$.

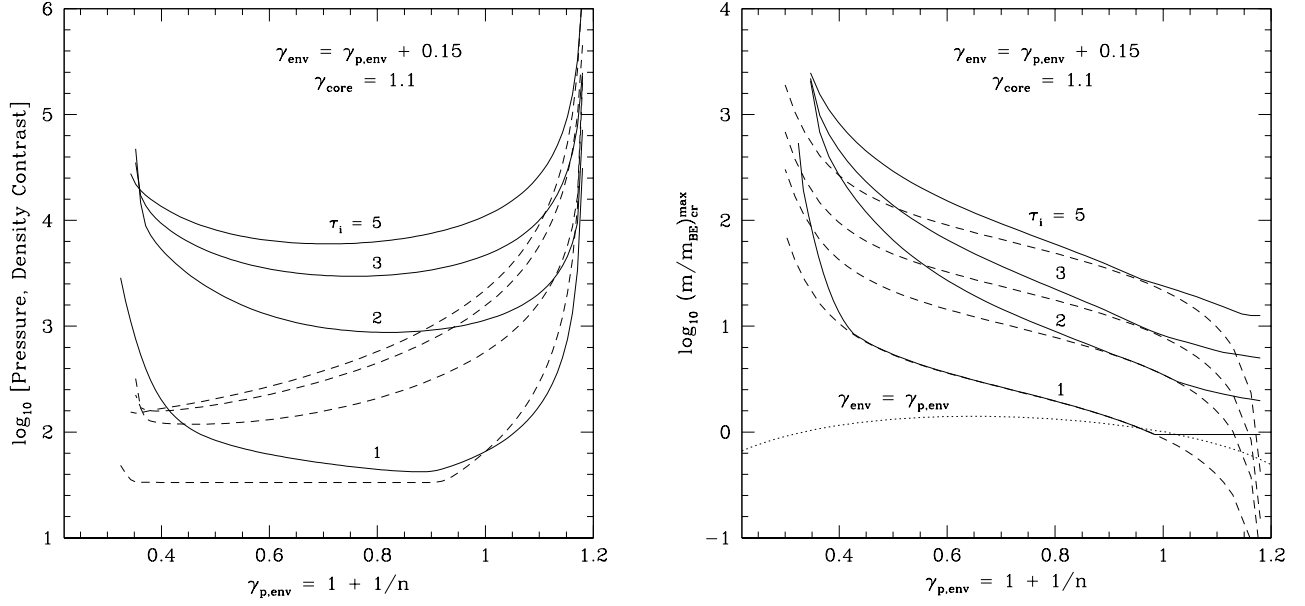


FIG. 10.— Properties of non-isentropic CPSs with $\gamma_{core} = 1.1$ and $\gamma_{env} = \gamma_{p,env} + 0.15$. (a) Maximum critical pressure (dashed curves) and density (solid curves) contrasts as a function of $\gamma_{p,env}$. Curves are labeled by τ_i . (b) Maximum critical masses as a function of $\gamma_{p,env}$ (solid curves). Also shown are the critical masses of pure polytropes with $T_{core} = \tau_i T_{core}(\tau_i = 1)$ (dashed curves). The dotted line shows the mass of isentropic polytropes.

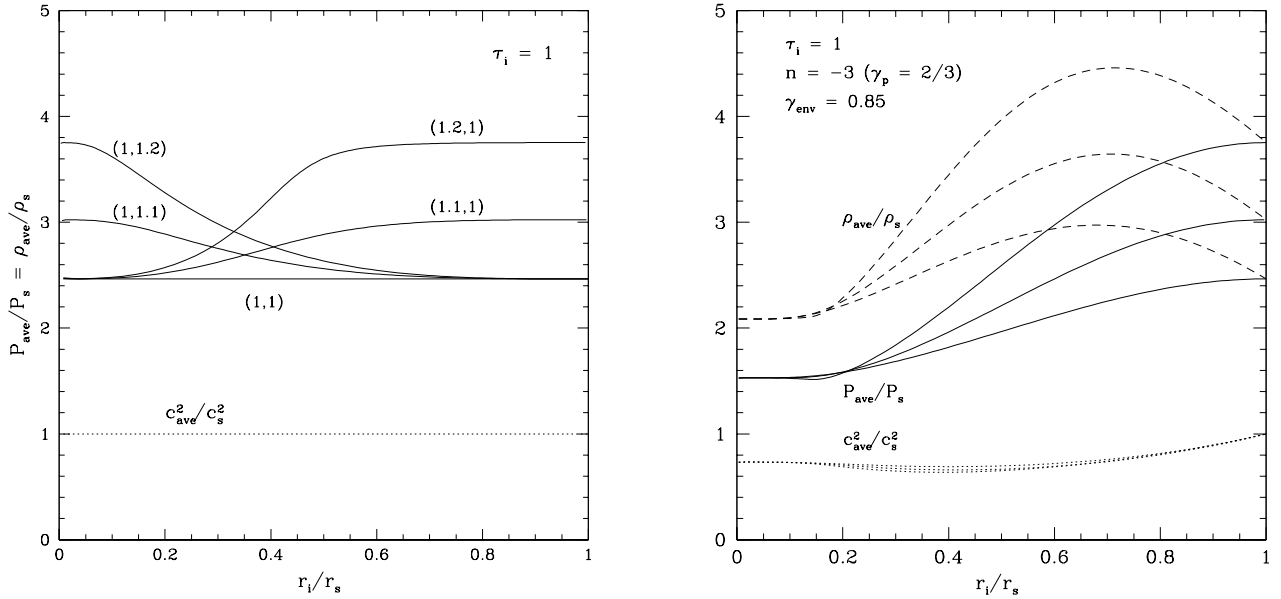


FIG. 11.— (a) Mean pressure contrasts (solid curves) as a function of fractional core radius in the $\tau_i = 1$, non-isentropic CIS. Each curve is labeled by its corresponding value of $(\gamma_{core}, \gamma_{env})$. The dotted line shows the mean sound speed contrast, which is equal to unity since $\tau_i = 1$. (b) Mean pressure contrasts (solid curves) in the $\tau_i = 1$, non-isentropic CPS with $n = -3$ and $\gamma_{env} = 0.85$. Mean density contrasts (dashed curves) and mean sound speed contrasts (dotted lines) are also shown. Within each set of curves, the corresponding value of γ_{core} is, from bottom to top, 1, 1.1, and 1.2.

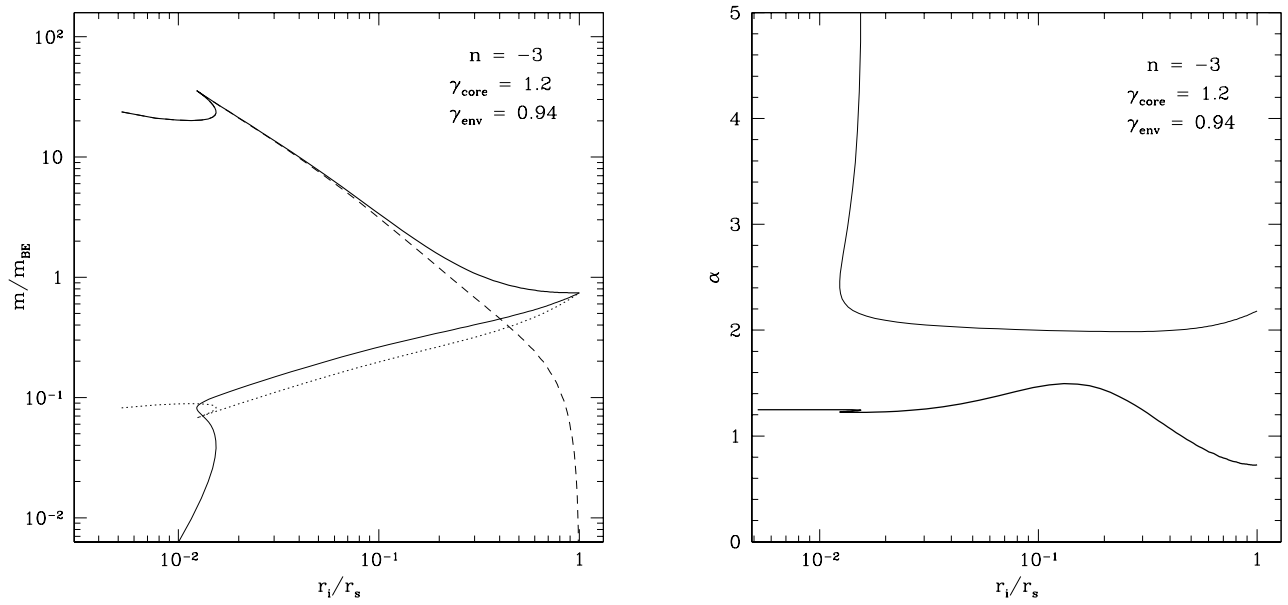


FIG. 12.— (a) Dimensionless masses of a critically stable, non-isentropic CPS with $\tau_i = 1$, as a function of the fractional core radius. The solid curve shows the core mass alone; the dashed curve, the envelope mass; and the heavy solid curve the total of the two. The dotted curve is the critical mass of the core alone. (b) Virial parameters for the core alone (solid curve) and the entire cloud (heavy solid curve). See text for details.